

University of Szeged
Faculty of Pharmacy
Institute of Pharmaceutical Technology and Regulatory Affairs
Head: Dr. habil. Ildikó Csóka PhD

Ph.D. thesis

**Investigation of physicochemical characteristics and tablettability of
titanate nanotube-active drug composites**

By
Barbara Sipos
Pharmacist

Supervisors:
Dr. Géza Regdon jr. PhD
and
Dr. Tamás Sovány PhD

Szeged
2019

ARTICLES RELATED TO THE THESIS

- I. **Sipos B.**, ifj. Regdon G., Sovány T.: *Titanát nanocsövek a gyógyászatban*. Acta Pharmaceutica Hungarica 85:(2) pp. 71-79. (2015)
IF: -
- II. **B. Sipos**, K. Pintye-Hódi, Z. Kónya, A. Kelemen, G. Regdon jr., and T. Sovány: *Physicochemical characterisation and investigation of the bonding mechanisms of API-titanate nanotube composites as new drug carrier systems*. International Journal of Pharmaceutics 518:(1-2) pp. 119-129. (2017)
IF: 3.862, Q1
- III. **B. Sipos**, G. Regdon jr., Z. Kónya, K. Pintye-Hódi, and T. Sovány: *Comparative study on the rheological properties and tablettability of various APIs and their composites with titatane nanotubes*. Powder Technology 321: pp. 419–427. (2017)
IF: 3.230, Q1
- IV. **B. Sipos**, K. Pintye-Hódi, G. Regdon jr., Z. Kónya, M. Viana, and T. Sovány: *Investigation of the Compressibility and Compactibility of Titanate Nanotube-API Composites*. Materials (Basel) 11:(12) p. 2582. (2018)
IF: 2.467, Q2

PRESENTATIONS RELATED TO THE THESIS

1. Sovány T., **Sipos B.**, Kónya Z., Hódi K., ifj. Regdon G.: Titanát nanócső-hatóanyag kompozitok, mint ígéretes, új hordozó rendszerek a gyógyászatban, MKE Kristályosítási és Gyógyszerformulálási Szakosztály 7. Kerekasztal Konferenciája, Szeged, 2014
2. Sovány T., **Sipos B.**, Sápi A., Kónya Z., Hódi K., ifj. Regdon G.: Diklofenak nátrium és diklofenak nátrium-titanát nanocső kompozit tartalmú tabletták tulajdonságainak összehasonlítása, XV. Congressus Pharmaceuticus Hungaricus, Budapest, 2014
3. T. Sovány, **B. Sipos**, A. Sápi, Z. Kónya, K. Pintye-Hódi, G. Regdon jr.: Comparison of the properties of the tablets containing diclofenac sodium or diclofenac sodium-titanate nanotube composite, 9th World Meeting on Pharmaceutics, Biopharmaceutics and Pharmaceutical Technology, Lisbon, 2014
4. T. Sovány, **B. Sipos**, Z. Kónya, K. Pintye-Hódi, G. Regdon jr.: Application of titanate nanotube composites for the modification of the solubility, dissolution kinetic and processability of drugs, 4th World Conference on Physico-Chemical Methods in Drug Discovery and Development, Rovinj, 2015
5. **B. Sipos**, T. Sovány, A. Sápi, Z. Kónya, K. Pintye-Hódi, G. Regdon jr.: Investigation of titanate nanotube-API composites as promising drug delivery systems, 1st European Conference on Pharmaceutics - Drug Delivery, Reims, 2015
6. **Sipos B.**, Sovány T., Kónya Z., Hódi K., ifj. Regdon G.: Titanát nanócső-hatóanyag kompozitok fizikai-kémiai tulajdonságainak vizsgálata, Gyógyszertechnológiai és Ipari Gyógyszerészeti Konferencia, Siófok, 2015
7. **B. Sipos**, T. Sovány, A. Sápi, Z. Kónya, K. Pintye-Hódi, G. Regdon jr.: Characterisation of titanate nanotube-active pharmaceutical ingredient (API) composites, 13th International Conference on Nanosciences & Nanotechnologies, Thessaloniki, 2016
8. **B. Sipos**, G. Regdon jr., K. Pintye-Hódi, T. Sovány: Structural characterisation and tablettability of diclofenac sodium-titanate nanotube composites, 4th World Congress and Expo on Nanotechnology and Materials Science, Barcelona, 2017
9. **B. Sipos**, T. Sovány, G. Regdon jr.: Comparison of the properties of tablets containing APIs or API-titanate nanotube composites, 6th FIP Pharmaceutical Sciences World Congress, Stockholm, 2017

TABLE OF CONTENT

1. Introduction.....	1
2. Aims.....	1
3. Literature Background	2
3.1. Synthesis methods of titanate nanotubes.....	2
3.2. Structural properties of free titanate nanotubes.....	4
3.3. Cytotoxicity of titanate nanotubes.....	4
3.4. Medical application of titanate nanotubes.....	5
3.4.1. Biosensors	5
3.4.2. Orthopaedic and dental implants.....	6
3.4.3. Drug delivery systems.....	7
3.4.4. Formulation challenges of titanate nanotubes.....	7
4. Materials and Methods.....	8
4.1. Materials.....	8
4.1.1. Active pharmaceutical ingredients	8
4.1.2. Excipients.....	9
4.2. Methods.....	10
4.2.1. Pre-formulation measurements	10
4.2.1.1. Morphological characterisation.....	10
4.2.1.2. Structure analysis	11
4.2.1.3. Physical properties	12
4.2.2. Formulation and in-die methods	13
4.2.2.1. Direct compression with excipients	13
4.2.2.2. Direct compression without excipients	14
4.2.3. Post-formulation methods	15
4.2.3.1. Out-of-die analysis of compaction	16
4.2.3.2. Tablet properties	17
5. results and discussion.....	19
5.1. Material properties: APIs, TNTs, API-TNT composites	19
5.1.1. Morphology.....	19
5.1.2. Surface free energy	20
5.1.3. Thermal properties	21
5.1.4. FT-IR.....	27
5.1.5. Powder rheology	31
5.1.6. Compressibility and compactibility	32
5.1.6.1. Energetic analysis	32
5.1.6.2. Post-compressional properties	35
5.2. Powder mixtures: APIs, API-TNT composites with excipients.....	37
5.2.1. Compressibility and compactibility	37
5.2.2. Tablet properties.....	39
5.2.2.1. Tablet density	39
5.2.2.2. Breaking force and tensile strength.....	40
5.2.2.3. Disintegration and drug dissolution	41
6. Conclusions.....	45
7. References.....	46

ABBREVIATIONS

API	active pharmaceutical ingredient
API-TNT	active pharmaceutical ingredient-titanate nanotube composite
ATN	atenolol
ATN+TNT	physical mixture of atenolol and titanate nanotubes
ATNTi	atenolol-titanate nanotube composite
DiltHCl	dilthiazem hydrochloride
DiltHCl+TNT	physical mixture of dilthiazem hydrochloride and titanate nanotubes
DiltTi	dilthiazem hydrochloride-titanate nanotube composite
DicNa	diclofenac sodium
DicNa+TNT	physical mixture of diclofenac sodium and titanate nanotubes
DicTi	diclofenac sodium-titanate nanotube composite
DSC	differential scanning calorimetry
FT-IR	fourier-transform infrared
HCT	hydrochlorothiazide
HCT+TNT	physical mixture of hydrochlorothiazide and titanate nanotubes
HCTTi	hydrochlorothiazide-titanate nanotube composite
MCW	mechanical energy
MS	mass spectroscopy
NCW	net energy
SEM	scanning electron microscopy
TCW	total energy
TEM	transmission electron microscopy
TGA	thermogravimetric analysis
ThCW	theoretical energy
TNT	titanate nanotube

1. INTRODUCTION

One of the key challenges of pharmaceutical industry is to find suitable methods to improve the processing, solubility and bioavailability of the available active substances. From this aspect, the rapidly developing nanotechnology captivated the attention of many medical scientists in recent years. Among others, organic and inorganic nanotubes got into the focus of their curiosity due to their promising properties presented in various scientific fields like physics, chemistry and electronics [1–4]. However, the strict safety requirements of medical applications shortly decreased the number of potential nanotube types for adaptation to medical use [5]. Despite the limiting factors, some inorganic nanotubes such as titanate nanotubes (TNTs) proved to be feasible for therapeutic use [6]. Thereafter several research works were engaged in the investigation of TNTs from the diagnostic to the active therapeutic fields. Considering that the term titanate nanotube covers TNTs with extremely diverse physicochemical properties (different tubular structure, length, drug carrying capacity, etc.), the unexplored medical aspects of TNTs is endless.

Regarding the pharmaceutical goals, the most essential and informative research topics over the safety questions are the capacity of TNTs to carry nano-sized active pharmaceutical ingredients (APIs), including the capability of TNTs to be loaded with active substances and the association methods stabilizing the API-TNT composites, as well as the processability and manufacturing of API-TNT composites.

2. AIMS

The purpose of the present research is to define the potential pharma-industrial benefits of the utilization of hydrothermally synthesized TNT carriers in the manufacturing and stabilization of nano-sized active substances. Within the confines of this purpose, the present study aims to thoroughly investigate and determine the physicochemical properties of API-TNT composites as well as to reveal the utility of composite formation in tableting with direct compression method.

The main endpoints of my research work are the followings:

- to determine the suitability of the API-TNT composite formation method
- to reveal the type(s) and strength of interactions inside the API-TNT composites

- to define the influence of composite formation on the physicochemical properties and behaviour of the API
- to estimate the effect of the composite formation on the formulation of tablets with direct compression and on the tablet properties
- to propose potential industrial utilization of TNTs

3. LITERATURE BACKGROUND

3.1. Synthesis methods of titanate nanotubes

The synthesis methods of titanate nanotubes may be classified into two big groups, the synthesis of surface attached and free TNTs. The synthesis of surface attached TNTs is commonly based on anodization method [7–9] and plays a key role in implantology, while the synthesis of free TNTs is mainly achieved by hydrothermal treatment of TiO_2 [10–14]. As the present research work is focusing on the utilization of free TNTs, the hydrothermal synthesis method will be presented in details.

Titanate nanotubes are synthesized of titania, a versatile material used for diverse applications such as medicine, cosmetics, paints, photocatalysis, etc. The first TNTs were synthesised by Hoyer in 1996 but the method which came into general use was documented by Kasuga et al. in 1998 and is known as alkali hydrothermal treatment [15, 16]. This method is widely used since it is easy, cheap and suitable for industrial-scale production [17]. Furthermore, the alkali hydrothermal treatment is tuneable for the structural parameters of the produced TNTs like the length or width which is also a huge advantage [18, 19]. Finally, this method is considered as eco-friendly due to its low energy need, the aqueous solution media and the closed system reaction way [20]. The considerable drawback of the method is its sensitivity to the synthesis conditions as pH, temperature and duration of treatment [21].

The flowchart of the alkali hydrothermal synthesis is displayed in Fig. 1. The synthesis process consists of two phases. In the first phase concentrated NaOH is added to the TiO_2 powder and this suspension is mixed for a certain time applying high temperature. As a result, some of the Ti-O-Ti bonds break up and Na^+ ions take place of Ti^+ ions creating Ti-O-Na and Ti-OH bonds in the system. Due to the electrostatic repulsion indicated by the charge of the Na^+ compound, TiO_2 nanosheets evolve [22]. The second phase is the acidic washing treatment with HCl. The acidic H^+ ions of HCl eliminate the Na^+ ions from the bonds forming Ti-OH and, due to the dehydration of the Ti-OH structures, Ti-O-

-H-O-Ti bonds are forming. As a result, the electrostatic repulsion disappears, and the superficial Ti-Ti bond length decreases facilitating the roll up of the nanosheets. As a last step, the charged components are eliminated from the system by a washing process with deionised water [23].

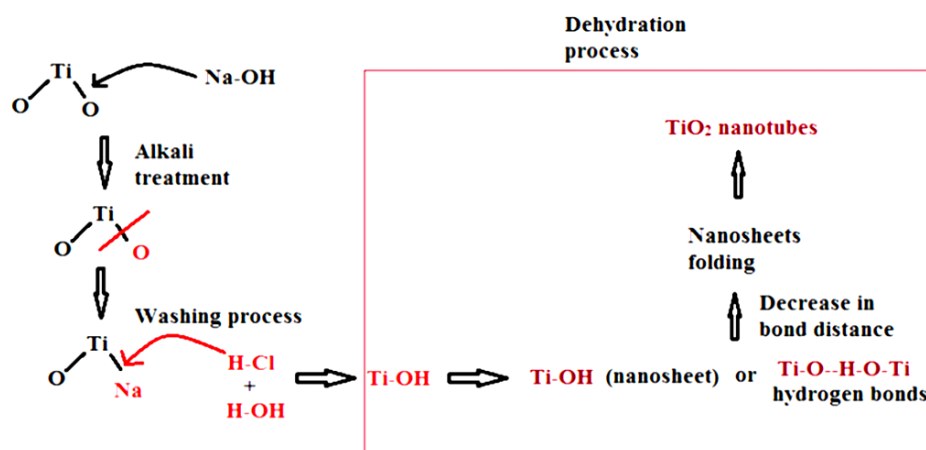


Figure 1. Formation mechanism of TNTs by alkali hydrothermal treatment [24]

The source material of the TNTs may be the different initial forms of TiO₂ powder the choice of which may influence the structural properties of the TNTs [20]. The synthesis setups also strongly affect the product quality which on one hand provides large liberty in product optimization while for the same reason demands careful and precise designing and implementation of the procedure [25, 26]. The most important statements to be considered are the followings: The optimal synthesis temperature is in the range of 100-180 °C since below 100 °C no nanotube formation can be expected while above 180 °C the nanotube formation slows down and nanorods appear instead [27, 28]. As for the optimal duration of the synthesis it has been revealed that on 150 °C the increase of stirring time from 2 hours to 72 hours increased the nanotube production from 0 % to 80 %. Accordingly the synthesis is normally accomplished in an autoclave under controlled temperature and/or pressure. The temperature is maintained above the boiling point of water to generate saturated vapour pressure. The pressure is modulated by the temperature and the aqueous solutions [20, 22].

It is notable that the mechanism of the tubular structure formation is still contested; a group of researchers believe that the nanotube formation is related to the hydrothermal phase while others find that the washing step is the precursor of the rolling-up of the nanosheets [22, 29]. Nevertheless, it is generally agreed that in alkaline conditions TiO₂

powders first transform into nanosheets and these intermediate nanosheets then roll up and form nanotubes [30].

3.2. Structural properties of free titanate nanotubes

As described in Section 3.1., hydrothermally synthesized TNTs are results of the scrolling of nanosheets and therefore have a special spiral cross-sectioned tubular structure (Fig. 2).

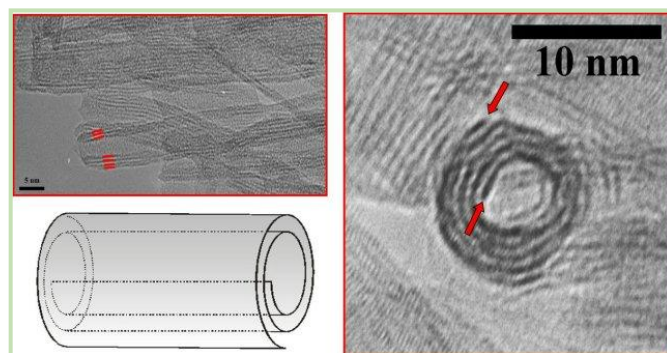


Figure 2. Schematic structure and TEM images of hydrothermally synthesized TNTs [31]

According to the formation mechanism, TNTs are asymmetric and open-ended on both sides. The geometry (length and diameter) of the TNTs can vary in large scale based on the synthesis parameters. As for the number of walls, the statistics show that TNTs generally possess five walls but TNTs with three or six walls could also be observed. Beside the structural parameters, it is important to highlight that TNTs show tendency to aggregate which is a common phenomenon of nanomaterials [32].

Due to the tubular structure, TNTs are suitable to be filled with or to carry nanosized drugs with therapeutic goals. The rolled-up structure allows the TNTs to expand in case of drug incorporation resulting in great drug carrier capacity [32]. Moreover, TNTs can also be functionalized with diverse agents which opens new directions in targeted drug delivery [33–38].

3.3. Cytotoxicity of titanate nanotubes

The non-toxicity of TNTs is an essential criterion of medical application. In case of nanomaterials the safety parameters are especially in the spotlight due to the limited knowledge of nanosized materials and the hardly measurable long-term effects. Based on the results documented so far TNTs show to be safe for human use [39–41]. However, it

is notable that, as the below examples also indicate, most of the cytotoxicity tests have been performed in vitro and in vivo studies are still underrepresented in the topic.

In a research of Fenyvesi et al. the toxic effect of TiO_2 and TNTs was tested on Caco-2 cells [42]. The cells were treated with different concentrations of TiO_2 and TNTs for 120 minutes. A 2% solution of Triton X-100 was used as a positive control in the study. The cell viability was measured with MTT tests. In contrast with the Triton X-100 solution which resulted in total cell destruction, the solutions of TiO_2 and TNTs did not show any change in cell viability up to 5 mg/ml concentration after 120 minutes. Another important examination was performed by Papa et al. who investigated not only the cytotoxicity but also the internalization pathways of TNTs on contractile cardiomyocyte monolayer [43]. Cytotoxicity was tested for pure and PEI-functionalized TNTs as well and no cytotoxic effect was recorded for either forms. As for the internalization of TNTs, the measurements revealed that TNTs pass through the cell membrane by diffusion and endocytosis which is in accordance with the results of other researchers.

3.4. Medical application of titanate nanotubes

The medical utility of TNTs has been widely investigated in the recent years. The main fields of the experiments were biosensors, implants and target therapies.

3.4.1. Biosensors

TNTs are good conductors, semi-conductors and show great catalytic and photoelectric properties. Accordingly, they can be used perfectly as electrochemical biosensors [44–47]. With the aim to diagnose Parkinson disease and to monitor neurotransmission procedures, an electrochemical biosensor has been developed by Liu et al. to measure the dopamine level in the extracellular fluid [48]. A stable TNT film has been created on a GC (glassy carbon) electrode. Since dopamine is positively charged in pH=7.4 buffer, it electrostatically approaches to the surface of TNTs covered by OH^- groups. The $-\text{NH}_2$ and OH^- functional groups of dopamine form hydrogen bonds with the OH^- groups of the TNT film. The dopamine molecules accumulate on the surface of the TNTs and some molecules may also get into the nanotubes. It can be stated, that the TNTs can preconcentrate the cationic dopamine in physiological conditions (pH=7.4) and therefore the dopamine shows a quasi-reversible redox peak on the surface of the TNT/GC electrode. The important advantage of this method compared to the already available ones

is that it is capable to detect dopamine selectively in the tissues beside the hardly separable ascorbic acid and uric acid which also give voltammetric signal.

3.4.2. Orthopaedic and dental implants

Nanomedical research shows huge interest in the application of TNTs in orthopaedic and dental implant therapies [49–71]. By the anodization technique TNTs with controlled parameters can be fabricated on pure titanium and titanium alloy surfaces (Fig. 3). The superficial TNT layer closely mimics the nanoscale architecture of the human bone which may provide ideal conditions for bone regeneration. Based on results of many researchers, titanium implants covered by TNTs accelerate the differentiation of mesenchymal stem cells into osteocytes resulting in fast bone regeneration and osteointegration. Besides, these implants can stimulate the osteoblasts and therefore enhance the osteogenesis and mineralization.

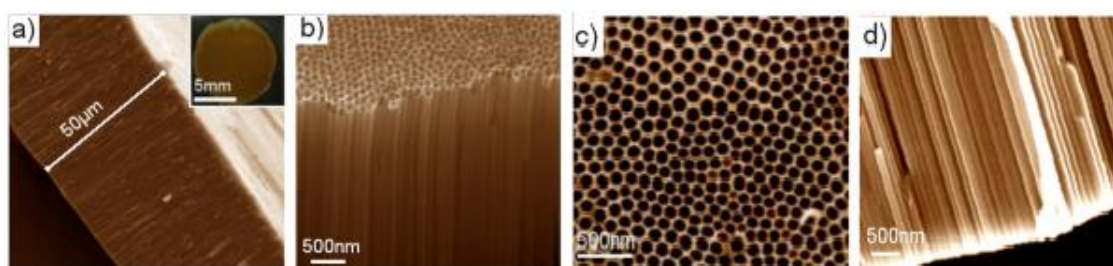


Figure 3. SEM images of TNTs fabricated by anodization of Ti in NH_4F /ethyleneglycol electrolyte: cross-sectional image (a), top surface (b, c) and bottom part (d) of the TNT layer. TNT layer was removed from the underlying Ti for imaging purposes [72].

Due to their tubular structure, the TNT coating can act as a drug delivery platform. By loading the TNTs with osteoinductive growth factors, anti-bacterial or anti-inflammatory drugs, increased osteointegration and prevention of peri-implant infections becomes available [73–82]. Moreover, if the loaded TNTs are covered with a biocompatible polymer film, controllable local drug release can be achieved as well [83–87]. A good example to all these functions was reported by Gulati et al. who synthesized a TNT layer on a titanium surface by anodization method and loaded the nanotubes with indomethacin [72]. To achieve a controlled drug release from the TNT layer, the surface of the implant was coated with biodegradable chitosan and PLGA (poly(lactic-co-glycolic acid)) by simple dip-coating method. According to the results, the polymer coat resulted in reduced burst release and extended the overall release. Dependent on the polymer thickness, the duration of drug release extended from 4 days to more than 30 days.

3.4.3. Drug delivery systems

Due to the flexible tubular structure and the favourable surface properties, TNTs can act as drug carriers either by drug incorporation and surface substitution therefore providing a large spectrum of drug delivery approaches. Based on their special properties, TNTs may efficiently be used in targeted therapies as well where the active substance is required to be directly delivered to the targeted cells [88, 89].

The focus of the examination of TNTs as drug delivery systems is cancer therapy [90–92]. It is known that the vascular structure of cancer cells is of high permeability with poor lymphatic system and therefore nanocarriers can easily get into the cells and release the API locally. For more effective and selective response, nanocarriers can also be functionalized with antibodies. Among others, Baati et al. reported about the promising targeted drug delivery activity of TNTs [93]. They investigated the safety of TNTs and cellular effect of genistein loaded TNTs on U87-MG cancer cell line. The measurements revealed the non-toxicity of the empty TNTs on the cells up to 100 µg/ml concentration. As regards the genistein loaded TNTs, the successful cellular uptake resulted in cytotoxicity and significant anti-migratory effect on the U87-MG human glioblastoma astrocytoma. Another interesting research work has been published by Loiseau et al. who investigated the antitumor activity of docetaxel-functionalized TNTs in vivo prostate tumour, in mice [94]. The intratumoral injection showed that more than 70% of TNTs were retained in the tumour for at least 7 days and that the tumour growth in mice receiving docetaxel in composite form with TNTs was significantly slower than in mice treated with pure docetaxel. These outstanding results may open new directions in cancer therapy in the future.

3.4.4. Formulation challenges of titanate nanotubes

The formulation of drug loaded and/or functionalized free TNTs is a completely new field in nanomedicine. As a result, in research works TNTs are commonly dispersed in certain liquids and are used as a simple solution. However, TNTs have the appearance of a powder which indicates that they could be formulated into many kinds of dosage forms depending on the therapeutic purpose. In practical terms, tablet formulation is certainly the most beneficial choice since tablet is still the most popular dosage form from patient compliance and pharma-industry aspects as well. In case of successful tableting, TNTs may provide an alternative to many other nanocarriers like liposomes, micelles,

dendrimers, etc., whose large-scale manufacturing and stabilization meet many difficulties [95].

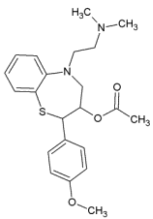
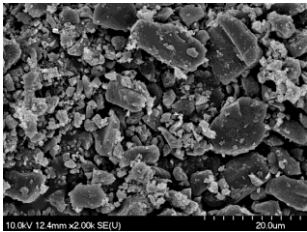
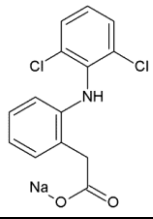
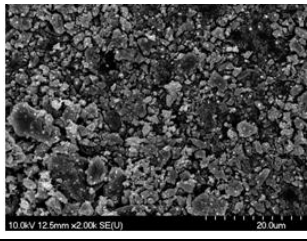
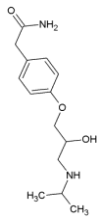
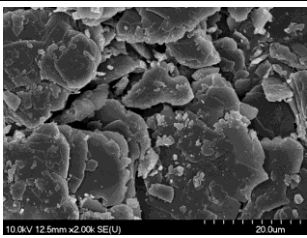
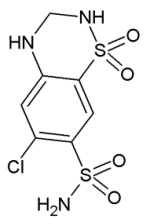
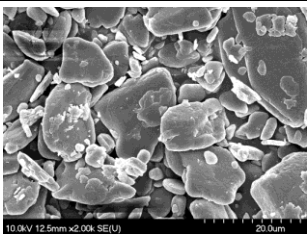
4. MATERIALS AND METHODS

4.1. Materials

4.1.1. Active pharmaceutical ingredients

A representative API of each Biopharmaceutical Classification System (BCS) classes was chosen for examination. Diltiazem hydrochloride (DiltHCl), diclofenac sodium (DicNa), atenolol (ATN) and hydrochlorothiazide (HCT) were supported by Sanofi-Aventis PLC, Hungary, Egis Pharmaceuticals PLC, Hungary, TEVA Pharmaceuticals PLC, Hungary and Gedeon Richter PLC, Hungary, respectively (Table 1).

Table 1. Materials applied for experimental work [96]

Name of API	Chemical structure	Scanning Electron Micrograph	BCS classification
Diltiazem hydrochloride (DiltHCl)			Class I. good solubility, good permeability
Diclofenac sodium (DicNa)			Class II. poor solubility, good permeability
Athenolol (ATN)			Class III. good solubility, poor permeability
Hydrochlorothiazide (HCT)			Class IV. poor solubility, poor permeability

Due to the character of the experimental work APIs were used in their regular crystalline form (Table 1) and in form of composites with titanate nanotubes (Fig. 4). 1:1 ratio of diltiazem hydrochloride-TNT (DiltTi), diclofenac sodium-TNT (DicTi), atenolol-TNT (ATNTi) and hydrochlorothiazide-TNT (HCTTi) composites were provided by the University of Szeged, Department of Applied and Environmental Chemistry. The formulation of the API-TNT composites was proceeded as follows. 1:1 ratio of API: 70% alcohol dissolution and the same 1:1 ratio of TNT:70% alcohol dispersion were prepared. After reaching a smooth dispersion of TNTs by 30 minutes of magnetic stirring, the two compositions were mixed and subjected to an hour-long ultrasonic treatment. Finally, the solvent was eliminated from the system in a vacuum dryer. The powder retained in this way contained the wanted API-TNT composites (Fig. 4) [96].

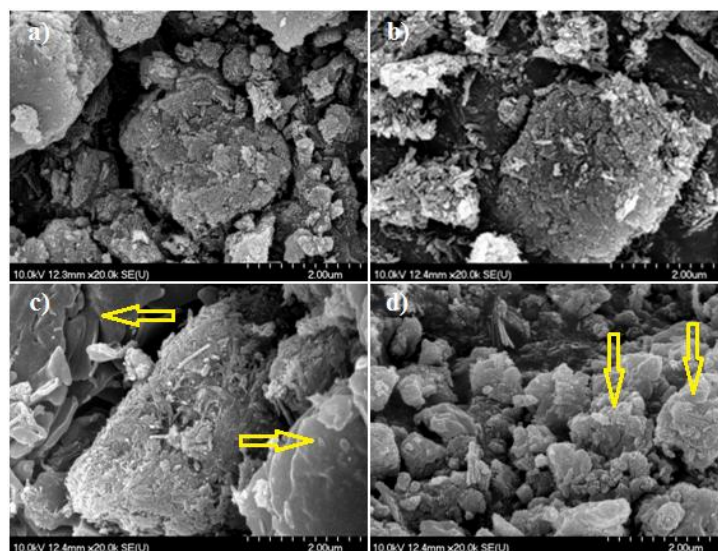


Figure 4. SEM images of the DiltTi (a), DicTi (b), ATNTi (c) and HCTTi (d)[96]

4.1.2. Excipients

Hydrothermally synthesized titanate nanotubes were produced by the University of Szeged, Department of Applied and Environmental Chemistry and were used for comparison and reference material in course of the experimental work. (Fig. 5)

Tableting was carried out with the use of the following excipients:

- Avicel PH 112 (FMC Biopolymer Inc., USA) is a microcrystalline cellulose product and is widely used as a binder for direct compression. Avicel PH 112 was expected to facilitate the compressibility of the raw materials and to provide appropriate tablet strength.

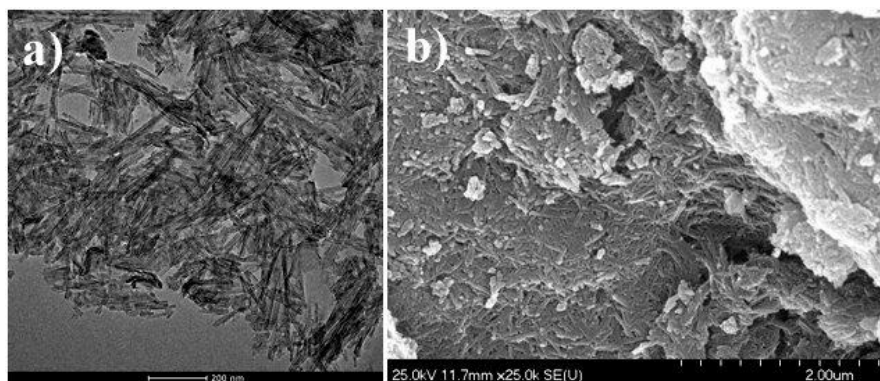


Figure 5. TEM micrograph (a) and SEM micrograph (b) of titanate nanotubes [96]

- Tablettose 70 (Meggler Pharma GmbH, Germany) is a product of agglomerated α -lactose monohydrate which has been developed especially for direct compression. Tablettose 70 was selected as a filler material due to its good flow properties and compressibility.
- Talc (Ph.Eur., Molar Chemicals Ltd., Hungary) is hydrated magnesium silicate and is a high functionality excipient in pharmaceutical formulations. In the present work talc was principally used for its glidant property.
- Magnesium stearate (Ph.Eur., Molar Chemicals Ltd., Hungary) is a powder with low surface free energy and is the most commonly used lubricant and antiadhesive excipient in solid dosage forms.

4.2. Methods

4.2.1. Pre-formulation measurements

APIs, TNTs and API-TNT composites were investigated in detail prior to formulation to reveal how composite formation affects the characteristics of the incorporated APIs.

4.2.1.1. Morphological characterisation

The morphology of the APIs, TNTs and API-TNT composites was investigated with a HITACHI S-4700 (Hitachi, Tokyo, Japan) scanning electron microscope. The samples were stuck to a carbon adhesive tape and were coated with a thin conductive golden layer by a Polaron E5100 (Polaron Ltd., VG Microtech, UK) sputter coating apparatus. The scanning electron microscopy (SEM) images were taken at a magnification of 2.0-25 k, using 25.0 kV of accelerating voltage for the TNTs and 10.0 kV for the APIs and the API-TNT composites. The air pressure was set to 1.3–13 MPa in all cases.

Besides the SEM imaging, TNTs were analysed with a FEI Tecnai G2 20 X-TWIN (FEI, Hillsboro, OR, USA) transmission electron microscope at 100 kV of accelerating voltage. The transmission electron microscopy (TEM) images did not only serve for texture analysis but also allowed to estimate the particle size of the TNTs by using Image J 1.47t (National Institute of Health, Bethesda, MD, USA) software.

4.2.1.2. Structure analysis

Thermogravimetric analysis (TGA) and Differential scanning calorimetry (DSC) tests of APIs, TNTs and API-TNT composites were performed with a Mettler Toledo TGA/DSC1 simultaneous analyser (Mettler-Toledo GmbH, Switzerland). To clarify the effect and advantages of composite formation, 1:1 ratio physical mixtures of TNTs and APIs (DiltHCl+TNT, DicNa+TNT, ATN+TNT, HCT+TNT) were also measured. Samples of 10 ± 1 mg weight were put and closed into a 100- μ l-volume aluminium pan. Samples were tested under rising temperature between 25 and 500 °C. Measurements were completed with a 10 K/min heating rate, using nitrogen as purge gas. The results were evaluated with STARe Thermal Analysis Software. Results were normalized to sample weight.

The DSC/TG analysis was complemented with mass spectroscopy (MS) measurements by using a ThermoStarTM GSD 320 (Pfeiffer Vacuum GmbH, Asslar, Germany) quadrupole MS connected to the Mettler Toledo TGA/DSC1 simultaneous analyser (Mettler-Toledo GmbH, Switzerland). The connection was assured by a silica capillary device, maintained at the heat of 120°C. Measurements were performed under N₂ atmosphere (purity: 99.999 %, flow rate: 70 mL·min⁻¹). As a first step, the characteristic peaks of the tested materials were screened from the evolved gases scanned in the range of 1-300 m/z. In this way, it was sufficient to take the subsequent measurements only on the selected m/z masses. Results were evaluated with Quadera and Star^e software.

A Thermo Nicolet Avatar 330 (Thermo Fisher Scientific Ltd., Waltham, MA, USA) Fourier transform infrared (FT-IR) spectrometer with a Transmission E. S. P. accessory was used to record FT-IR spectra of the APIs, TNTs and API-TNT composites. The spectrometer performed 256 scans at a resolution of 4 nm with H₂O and CO₂ corrections. Results were evaluated with EZ OMNIC software. For the easier understanding of the results, the signals of TNTs were subtracted from the spectrum of the API-TNT composite. Therefore, the spectra of native and incorporated API could be plotted

together and compared. The spectra for comparison were normalized to the highest peak, usually belonging to C=O stretching.

4.2.1.3. Physical properties

The surface free energy of the APIs, TNTs and API-TNT composites was studied with a DataPhysics OCA 20 (DataPhysics Instruments GmbH, Filderstadt, Germany) optical contact angle tester. 13-mm-diameter tablets were prepared from the tested materials with a Specac hydraulic press (Specac Ltd., Orpington, UK) at a pressure of 4 tons. According to the sessile drop method, a polar (water) and an apolar (diiodomethane) test liquid were dropped onto the surface of the samples. The known surface tensions of the test liquids allowed to calculate the disperse and polar components of the samples by applying the Wu equation (Eq. 1):

$$(1 + \cos \theta) \gamma_L = \frac{4\gamma_L^{Disp} \gamma_S^{Disp}}{\gamma_L^{Disp} + \gamma_S^{Disp}} + \frac{4\gamma_L^{Pol} \gamma_S^{Pol}}{\gamma_L^{Pol} + \gamma_S^{Pol}} \quad (1)$$

where θ is the contact angle between the test liquid and the solid phase, γ_L and γ_S are the surface tensions of the liquid and the solid phase in mJ/m², and *Disp* and *Pol* refer to the disperse and the polar components of the surface tension.

The surface free energy (γ^{TOT} (mJ/m²)) was calculated as the sum of γ^{Dis} and γ^{Pol} (Eq. 2):

$$\gamma^{TOT} = \gamma^{Disp} + \gamma^{Pol} \quad (2)$$

The polarity was defined by the following equation (Eq. 3):

$$Polarity (\%) = (100\gamma^{Pol})/\gamma^{TOT} \quad (3)$$

A software-controlled PTG-1 (PharmaTest Apparatebau AG, Germany) powder rheological tester was used to investigate the flowing properties of the APIs and API-TNT composites. A stainless-steel funnel with an opening outlet nozzle of 10 mm in-diameter was filled with 100 ml of powder. The powder flow through the nozzle was detected by inbuilt IR sensors. The apparatus provided information about the flow time and the angle of repose of the powder heap. All samples were measured in triplicate.

Densification of the APIs and the API-TNT composites were tested with a STAV 2003 Stampfvolumeter (Engelsmann AG., Germany). 250 ml of powder was put carefully into a graduated cylinder avoiding the powder packing. Bulk density was calculated from this powder volume. The cylinder filled with powder was then mechanically tapped by the apparatus at a speed of 1/sec until no further decrease in volume could be observed or

until the 1250 tap number was reached. Tap density was calculated from the stabilised, densified powder volume. The defined bulk density and tap density values were used to calculate the Hausner Ratio (Eq. 4) and Compressibility Index (Eq. 5) of the samples:

$$\text{Hausner Ratio} = \rho T / \rho B \quad (4)$$

$$\text{Compressibility Index} = [(\rho T - \rho B) / \rho T] * 100(\%) \quad (5)$$

where ρT is the tap density and ρB is the bulk density of the powder in g/cm^3 . Results were evaluated according to the United States Pharmacopeia (USP) scale of flowability [97, 98].

4.2.2. Formulation and in-die methods

Direct compression of the APIs and API-TNT composites without excipients was achieved to understand the behaviour of the raw materials during compression and thus to estimate their suitability for tableting with direct compression, while tableting with excipients aimed to demonstrate the industrial formulation of the materials and to prove the eligibility of the resulted API-TNT tablets on the market.

4.2.2.1. Direct compression with excipients

By using the appropriate excipients, formulations (Table 2) of APIs and API-TNT composites were compressed into tablets with direct compression.

Table 2. Composition of API and API-TNT tablets [96, 98]

Component	API tablets (300 mg)	API-TNT tablets (300 mg)
API (DiltHCl/DicNa/ATN/HCT)	16.7 %	-
API-TNT composite (DiltTi/DicTi/ATNTi/HCTTi)	-	33.3 %
Avicel PH 112	50.0 %	39.5 %
Tablettose 70	29.3 %	23.2 %
Talc	3.0 %	3.0 %
Magnesium-stearate	1.0 %	1.0 %

Tablets were prepared with constant tablet weight (300 mg) and quantity of API (50 mg) in order to be able to compare the API and API-TNT tablets according to the pharmaceutical requirements. The powders were mixed with a Turbula mixer (Willy A. Bachofen Maschinenfabrik, Switzerland) at 50 rpm for 8 minutes without magnesium-stearate and for 2 minutes more with it. The tablets were compressed with a Korsch EKO (E. Korsch Maschinenfabrik GmbH, Berlin, Germany) eccentric tablet press,

instrumented with strain gauges and a displacement transducer. 10 mm-diameter flat punches were applied with a compression force of 5.0, 7.5, 10.0, 12.5 and 15.0 kN for all compositions [98]. Batches of at least 50 tablets per composition per compression pressure were produced.

4.2.2.2. Direct compression without excipients

Tableting of the raw materials (TNTs, APIs and API–TNT composites) without excipients was achieved with a Lloyd 6000R uniaxial press (Ametek SAS Lloyd Inst, Elancourt, France), instrumented with a force gauge and a linear variable differential transformer extensometer. The compacts were prepared in a 1 cm³ stainless steel cell with manual filling, using 50, 100, 150, 200 and 250 MPa pressures for each material. The weight of the powder was determined using the bulk density of the unpacked powders. At least 3 tablets per compression pressure were made from each component, with a tableting punch speed of 1 mm/sec [99].

Due to the built-in sensors, the Lloyd 6000R uniaxial press (Ametek SAS Lloyd Inst, Elancourt, France) equipment allowed the thorough investigation of the behaviour of the raw materials under compression pressure via the in-die analysis of compaction.

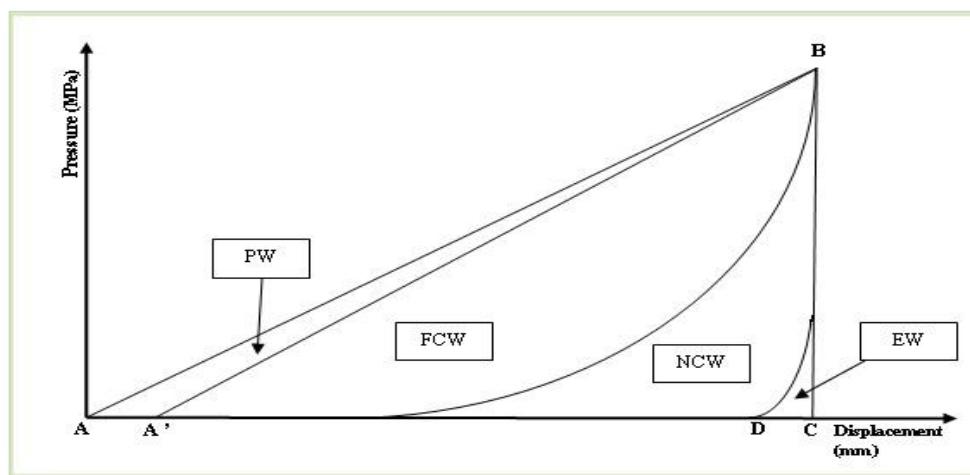


Figure 6. Schema of the compression cycle [99]

Force and displacement data were recorded by a computer (R-Control software, Version 2.0, Lloy Inst LTD, Fareham, UK) connected to the equipment. The retrieved data set was evaluated with Origin 7.5 software (OriginLab Corporation, Northampton, MA, USA) in order to determine the energy utilisation of the raw materials during the compression cycle (Fig. 6, Table 3). With the aim of estimating

linear interrelations between different energies and their changes in the applied compression pressure range, energies were normalised to compact weight.

Table 3. Energies associated to the compression cycle [99]

Type of energy	Area of compression cycle	Usage of energy
Packing energy (PW)	ABA' area	Initial packaging of the particles
Theoretical energy (ThCW)	A'BC area	Powder compaction
Net energy (NCW)	A'BD curve	Plastic deformations
Friction energy (FCW)	A'BA' curve	Particle–particle and particle–die frictions during densification
Elastic energy (EW)	DBC curve	Elastic deformations
Interrelations		
Mechanical energy (MCW)	ABC area	MCW=PW+FCW+NCW+EW; MCV=ThCW+PW
Total energy (TCW)	A'BC curve	TCW=NCW+EW; TCW=ThCW- FCW

The energy analysis was expanded with the determination of R_i (R_1 , R_2 and R_3) values which serve to describe pressure related transformation of energies: MCW into ThCW (R_1), ThCW into TCW (R_2) and TCW into NCW (R_3). R_i values were calculated as follows (Equations 6-8):

$$R_1 = \Delta \text{ThCW} / \Delta \text{MCW} \quad (6)$$

$$R_2 = \Delta \text{TCW} / \Delta \text{ThCW} \quad (7)$$

$$R_3 = \Delta \text{NCW} / \Delta \text{TCW} \quad (8)$$

Each R_i yield refers to one of the 3 big phases of the compression cycle. R_1 shows the packaging ability of the materials, R_2 is indicative of the frictions and R_3 displays the plasticity of the materials.

4.2.3. Post-formulation methods

All post-formulation investigations have been carried out to confirm the effects of API-TNT composites on tablet properties and to approve the results of the compressibility and compactibility studies.

4.2.3.1. Out-of-die analysis of compaction

The compaction properties of the powder mixtures (Table 2) were estimated with the commonly used Kawakita and Walker out-of-the die models.

The Kawakita equation (Eq. 9) was used to study the particle rearrangement of the powder mixtures during the packaging phase of the compression:

$$P/C = P/a + 1/ab \quad (9)$$

where P is the applied pressure in MPa, C is the degree of the volume reduction and a and b are constants. The degree of volume reduction is expressed by Eq. 10:

$$C = (V_0 - V)/V_0 \quad (10)$$

where V_0 is the initial volume of the powder bed and V is the volume of the powder bed at the applied pressure in mm^3 . Constant a indicates the initial porosity of the sample. Its higher value presumes loose packing of the powder in the die before compression. Constant $1/b$ describes the pressure that is needed to reduce the powder bed volume by 50%. Higher coefficient $1/b$ implies higher cohesive energy of interaction, which shows up as a hindered particle rearrangement.

The behaviour of the powder mixtures in the deformation phase of the compression was investigated using the Walker (1923) equations (Eqs. 11 and 12):

$$\log P = -LV + C_1 \quad (11)$$

$$100V = -W \log P + C \quad (12)$$

where P is the applied pressure in MPa, L is the pressing modulus which reflects the volume reduction at a given pressure, V is the relative volume, W is the Walker coefficient which gives information about the volume reduction corresponding to logarithmic increment in the pressure, and C and C_1 are constants. The relative volume is expressed by Eq. 13:

$$V'/V_0 \quad (13)$$

where V' is the volume at the applied pressure and V_0 is the initial volume of the powder bed in mm^3 [98].

4.2.3.2. Tablet properties

Geometrical parameters of tablets were measured with different methods in case of tablets produced with and without excipients for technical reasons (Table 4)

Table 4. Determination methods of geometrical parameters of tablets

	Tablets produced with excipients	Tablets produced without excipients
Mass (m) tester	Kraemer UTS-50 tablet tester (Charles Ischi AG, Switzerland)	analytical scale
Height (h) tester		Calliper
Diameter (d) tester		Lloyd 6000R uniaxial press (Ametek SAS Lloyd Inst, Elancourt, France)
Timing of measurement	right after production and 1 week after production	24 hours after production
Number of measured tablets/composition/compression force	minimum 20	minimum 3

The compaction ratios (ρ , %) of the tablets fabricated without any excipients were determined using the following equation (Eq. 14):

$$\rho = (d_{\text{compact}}/d_{\text{initial}}) \times 100 \quad (14)$$

where d_{compact} is the tablet density after ejection and d_{initial} is the initial or bulk powder density, both in g/cm^3 . The tablet density was calculated from the geometrical parameters ($m/\pi h(d/2)^2$), while the bulk density was determined as described in Section 4.2.1.8.

Similarly to the investigation of geometrical properties, braking force of the tablets fabricated with and without excipients were studied using different methods (Table 5).

Table 5. Examination methods of breaking forces of tablets

	Tablets produced with excipients	Tablets produced without excipients
Breaking force tester	Heberlein 2E/205 tablet hardness tester (HeberleinAG, Switzerland)	Lloyd 6000R uniaxial press (Ametek SAS Lloyd Inst, France)
Number of tested tablets /composition/compression force	10	3

From the breaking force and the geometrical properties the tensile strength could be defined as follows (Eq. 15):

$$\sigma = 2F/(\pi * d * h) \quad (15)$$

where σ is the tensile strength in MPa, F is the breaking force in N, d is the diameter and h is the height of the tablet in mm.

The texture of the breaking surface of the tablets compressed with the use of excipients was investigated with a Hitachi S4700 (Hitachi Ltd., Japan) scanning electron microscope. Prior to imaging, the samples were stuck to a double sided carbon adhesive tape and were covered with a thin conductive golden coating layer created by a Polaron E5100 (Polaron Ltd., VG Microtech, UK) sputter apparatus. Micrographs of the prepared samples were taken at a magnification of 100-500, using 10.0 kV of electron energy and 1.3-13 MPa of air pressure.

Disintegration was determined for tablets fabricated with excipients (Table 2) at all applied compression pressure. The disintegration tests were performed in distilled water according to the criteria of the European Pharmacopoeia [100]. Examination was accomplished with an Erweka ZT71 (Erweka GmbH, Germany) disintegration tester apparatus.

Drug dissolution was examined from tablets produced with excipients (Table 2). Tablets compressed with 5.0, 7.5, 10.0, 12.5 and 15.0 kN compression force were investigated for all compositions.

The drug release was determined with an Erweka DT700 (Erweka GmbH, Heusenstamm, Germany) dissolution tester, applying paddle method with a paddle speed of 100 rpm. The dissolution was tested at 37°C in pH 1.2 enzyme free artificial gastric juice and pH 6.8 phosphate buffer media. Aliquots of 5 mL were taken after 3, 5, 10, 15, 30 and 60 minutes. The released drug concentrations were determined with a ThermoScientific GENESYS 10S UV-VIS spectrophotometer (Thermo Fisher Scientific Ltd., Waltham, MA, USA).

5. RESULTS AND DISCUSSION

5.1. Material properties: APIs, TNTs, API-TNT composites

5.1.1. Morphology

As presented in the Section 2.2.1., the hydrothermally synthesized TNTs have a special and well definable appearance due to the formation mechanism.

The TEM and SEM images (Fig. 5) confirmed the expected texture of the TNTs although the method was not suitable to reveal the inside layers of the spiral cross-sectioned tubular structure. Based on the TEM pictures, the average diameter of the TNTs was determined to be 7.01 nm (SD \pm 1.08 nm) while the length, which is a matter of the synthesis parameters, was found to be 164.25 nm (SD \pm 50.38 nm). The SEM pictures allowed concluding that TNTs are not present individually but in form of aggregates. Instead of an arrangement along the length of the nanotubes, the SEM images revealed disorderly arranged TNTs forming loose aggregates. Aggregation is a well-known phenomenon for nanomaterials which may affect their application in a positive or a negative way. On the present work aggregation has a definitely positive influence since it increases the flowability and in parallel decreases the adhesivity of the TNT powder, without any negative effect on the behaviour of the incorporated drug. Moreover, the loose aggregate structure is also advantageous as it provides good processability and therefore will not limit any formulation procedure. The effect of drug incorporation on the pure TNTs and the morphological characteristics of the API-TNT composites could be defined by comparing the SEM images of the APIs (shown in Table 1), TNTs (Fig. 5) and API-TNT composites (Fig. 4).

As concerns the TNTs, it is remarkable that the nanotubes thickened due to the incorporation. This proves the rolled-up structure that lends flexibility to the nanotubes and allows the necessary expansion to enclose drug particles, and refers to the APIs being located not only in the central channel of the TNTs but between the walls as well. Nevertheless, SEM pictures revealed that APIs may be found also on the surface of the TNTs in a certain association with the superficial hydroxyl groups that densely cover the TNTs (Fig. 7). Furthermore, SEM images of the composites revealed that the efficacy of drug incorporation was not equal for all 4 APIs. While the composite formation of DiltHCl and DicNa seemed to be ideal and resulted in homogenous composite products, that of ATN and HCT was only partially effective and left several individual API crystals

in the final products, as shown by yellow arrows on Fig. 4. Based on the pictures, the ATNTi product seems like the physical mixture of the source materials, while in case of the HCTTi product, a kind of reverse mechanism of the composite formation could be recognized inducing that approx. 60% of the API crystals are covered with TNTs [96].

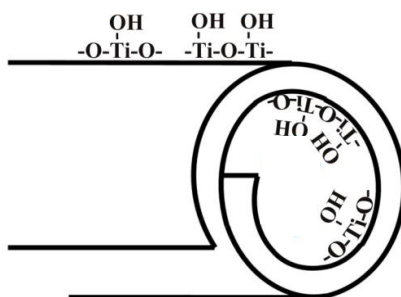


Figure 7. Presumed bonding sites of TNTs

5.1.2. Surface free energy

The surface characteristics of a material play a key role in its reactivity and basically determine its behaviour in any kind of formulation procedure. The determination of the surface characteristics of the materials aimed to gain additional information about the intermolecular interactions between the TNTs and the APIs within the composites [96].

As displayed in Table 6,

Table 6. Surface characteristics of TNTs, APIs and API-TNT composites [98]

Material	γ^{TOT} (mJ/m ²)	SD	γ^{Disp} (mJ/m ²)	SD	γ^{Pol} (mJ/m ²)	SD	Polarity (%)
TNT	80.72	±0.64	43.78	±0.54	36.94	±0.35	45.76
DiltHCl	78.60	±0.91	42.27	±0.72	36.33	±0.57	46.22
DiltTi	76.66	±1.56	42.22	±1.08	34.43	±1.12	44.91
DicNa	79.49	±1.00	42.58	±0.92	36.91	±0.40	46.43
DicTi	64.99	±1.95	44.02	±0.72	20.08	±1.80	30.89
ATN	59.48	±3.99	36.70	±2.96	22.77	±2.68	38.20
ATNTi	60.14	±4.25	40.45	±1.48	19.68	±3.87	32.72
HCT	69.51	±2.71	43.33	±0.79	26.18	±2.59	37.60
HCTTi	78.25	±0.86	44.65	±0.57	33.60	±0.64	42.93

TNTs have high surface free energy confirming their expected hydrophilic nature. This character of the TNTs is reflected in the γ^{TOT} values of the ATNTi and HCTTi composites which showed increment in this value in comparison with the pure ATN and HCT, respectively, which is in accordance with the SEM observations, where the individual

API crystals, partially covered by TNTs were identified, due to incomplete composite formation. However, this increment of γ^{TOT} value cannot be considered as substantial for ATNTi, due to the high SD of the results, which strengthens the physical mixture like behaviour of ATNTi. Overall, the increment in γ^{TOT} may be attributable to the surface coverage of the API crystals with TNTs, and the extent of increment is considered as an indicative of the ratio of the surface coverage. As regards the DiltTi and DicTi composites, a decrease of γ^{TOT} value and polarity could be noticed in comparison with both the TNTs and the pure APIs (DiltHCl and DicNa, respectively) as shown in Table 6. This finding confirms the successful incorporation of DiltHCl and DicNa and that the APIs are not only located in the internal part of the nanotubes but are also bonded to the surface. The decrease of γ^{TOT} and polarity indicates hydrophilic intermolecular interactions on the surface of the TNTs inducing the enrichment of the hydrophobic molecular parts on the particle surface. The higher decrease in surface free energy suggests a greater bonding ratio on the surface of the TNTs [96].

5.1.3. Thermal properties

The main focus of the further examinations was to reveal the interactions inside the composites in order to better understand their behaviour in formulation and post-formulation processes.

As a first step, thermal properties of pure TNTs were studied as common and basic component of all composites. TNTs showed to be thermostable in the measured range (Fig. 8). However, a moderate 11.66 % of weight reduction was detected between 30 °C and 340 °C. This was identified by MS as simple loss of water which partially may be the leftover of the washing step of synthesis process, or absorbed water vapour. Considering the big temperature range of water loss it can be established that water is not only adsorbed on the surface but is also located in the interior of the TNTs. The surface-adsorbed water evaporates in the range of 60-100 °C, while water loss in higher temperatures is attributable to the elimination of water from the internal parts of TNTs. It must be noted that no similar signals were detected in any of the composites which suggests that in the competition for the binding sites of nanotubes APIs take the place of the water molecules and create some kind of interaction with the TNTs [96].

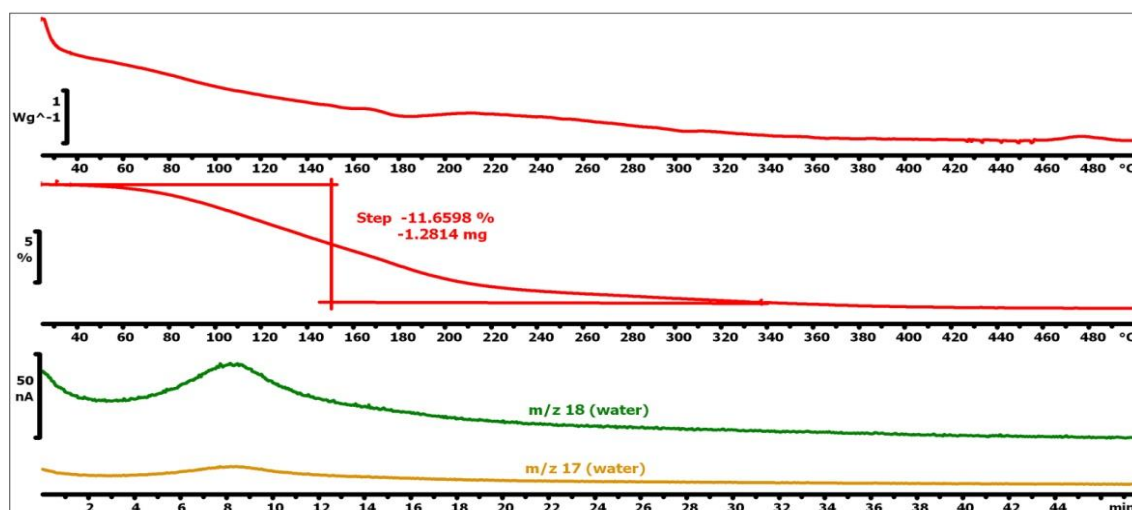


Figure 8. DSC, TG and MS curves of TNT [96]

To understand the interactions inside the composites, the thermal properties of the APIs were assessed together with the related API+TNT physical mixtures and API-TNT composites.

Table 7. Thermal parameters of APIs, API-TNT composites and API+TNT mixtures [96]

Sample name	Melting range (°C)	Melting point (°C)	Enthalpy of fusion (J g ⁻¹)	Weight loss (%)
DiltHCl	217.1-227.2	223.0	-118.45	83.34
DiltTi	187.3-208.7	201.0	-25.14	43.85
DiltHCl+TNT	192.7-212.1	204.3	-18.71	42.62
DicNa	290.3-297.8	295.2	-95.86	40.03
DicTi	258.8-271.5	264.5	-59.18	32.98
DicNa+TNT	289.5-297.6	292.5	-61.37	31.43
ATN	157.5-166.7	162.7	-148.75	78.25
ATNTi	155.9-166.5	161.0	-50.71	39.53
ATN+TNT	153.9-167.5	161.2	-55.30	39.15
HCT	269.6-281.7	274.8	-130.25	59.23
HCTTi	242.5-264.1	257.2	-46.66	34.27
HCT+TNT	266.3-277.1	272.5	-43.45	37.85

DiltHCl+TNT and DiltTi exhibited melting points at lower temperatures with broadened melting ranges and smaller relative fusion enthalpies in comparison with DiltHCl (Fig. 9, Table 7). Another difference is that the decomposition related peaks of DiltTi and DiltHCl+TNT do not appear clearly on the DSC curves, which is probably due to the approach of the endothermic and exothermic events resulting in the extinction of the opposite peaks (Fig. 9). This theory was confirmed by the TG-MS measurements where mass loss and peaks in ion current curves could be detected in the range of 220-420 °C.

The evaluation of DTG and MS results also revealed that TNTs prolong the decomposition independently to be in physical mixture or composite form. When comparing DiltTi and DiltHCl+TNT, the only remarkable difference was noticed between the DTG curves, where the decomposition peak of DiltTi appears with a time lag compared to DiltHCl+TNT (Fig. 9), which may indicate that in contrast with DiltHCl+TNT, the API is mainly found inside the nanotubes in DiltTi [96].

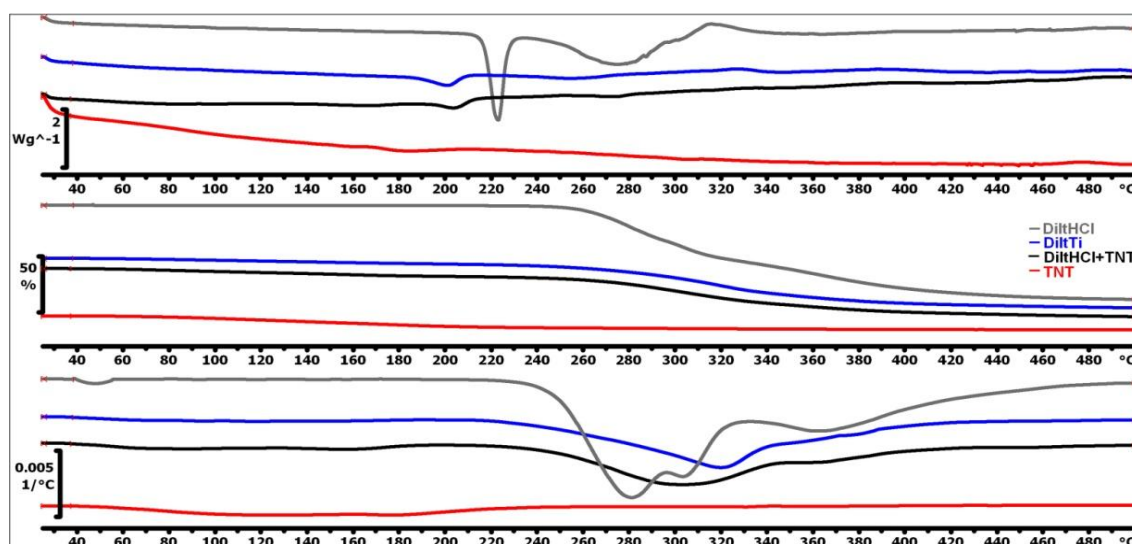


Figure 9. DSC, TG and DTG curves of DiltHCl, DiltTi, DiltHCl+TNT and TNT [96]

As regards the thermal properties of DicNa, DicNa+TNT and DicTi (Fig. 10), DSC curves of DicNa and DicNa+TNT were found to be similar in shape, but DicNa+TNT shows a slight shift of the peaks to lower temperatures indicating simultaneous fusion and decomposition (Table 7). Besides, the DTG curve of DicNa+TNT displayed mass loss in only one step, in contrast with the two decomposition steps of DicNa but the MS measurements confirmed the same evolved ion fragments for both samples. In contrast, the melting point of the incorporated DicNa strongly shifted to lower temperature and displayed a broader melting range in the DicTi composite (Table 7). Moreover, the decomposition of DicTi appeared as a flat and wide exothermic event. This difference clearly reveals itself on the DTG curves as well: although the thermal decomposition of DicTi occurred in two steps just like in the case of DicNa, these steps were manifested with different peak shapes and a shift to smaller temperatures, corresponding to the DSC curve [96]. While reviewing the evolved ion fragments belonging to the characteristic peaks (Table 8) it turned out that beside H_2O ($m/z=18, 17, 20$) and CO_2 ($m/z=44, 16, 12$,

45, 22), which were detected for all the samples, an extra gas release could be identified in the case of DicTi at 69 °C.

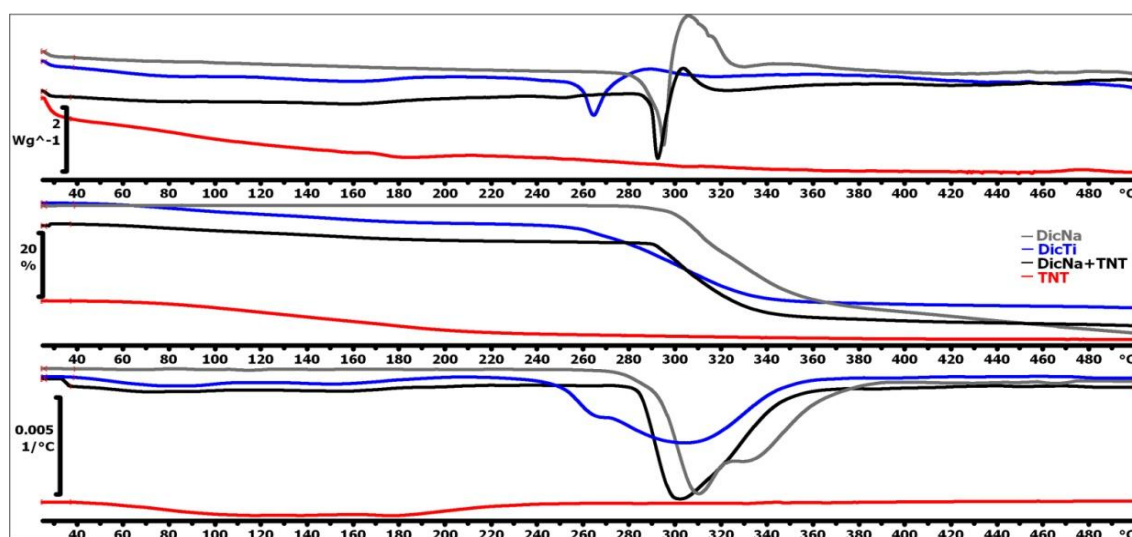


Figure 10. DSC, TG and DTG curves of DicNa, DicTi, DicNa+TNT and TNT [96]

The evolution of $m/z=31$ ion probably represents the detachment of the acetic acid functional group of DicNa. Taking into account that $m/z=31$ ion current was detectable only for DicTi, considerable interaction is assumable between the acid functional group of DicNa and the TNTs which shifts the electron structure of the DicNa molecule and therefore results an easier detachment of the acetic acid group from the molecule [96].

Table 8. Characteristics for the evolution of gases of DicNa, DicTi and DicNa+TNT. T1 is the temperature at the first peak of the gas evolution [96]

	Mass (m/z)	12	16	17	18	20	22	31	44	45
DicNa	Evolution range (°C)	314-388	289-396	284-386	284-392	292-368	310-376		299-395	314-385
	T1 (°C)	334	335	317	317	316	333		333	337
	Intensity of T1 (A)	2.25E-10	1.69E-09	1.23E-08	4.75E-08	1.19E-10	3.08E-11		1.95E-09	2.49E-11
DicTi	Evolution range (°C)				258-342			38-106	287-316	55-116
	T1 (°C)				267			69	302	62
	Intensity of T1 (A)				7.72E-08			1.14E-10	5.37E-10	2.64E-11
DicNa+TNT	Evolution range (°C)	305-331		289-354	288-345	291-322	303-323		298-330	
	T1 (°C)	315		300	296	296	313		312	
	Intensity of T1 (A)	1.19E-10		1.04E-08	4.04E-08	9.48E-11	1.32E-11		5.16E-10	

The comparison of the thermal behaviour of ATN, ATNTi and ATN+TNT samples displayed almost no differences (Fig. 11, Table 7). Fusion and thermal decomposition of all compounds occurred in a very similar way and the evolved ion fragments stated

conformity for all samples as well. The hard recognisability of the decomposition events of ATNTi and ATN+TNT in the DSC curves are only due to the relatively smaller quantity of API in ATNTi and ATN+TNT samples. Although the DTG curves showed extended decomposition for the nanotube containing samples, it is clear that this phenomenon is due to the nanotube itself and ATN is not capable of forming important interactions with TNTs [96].

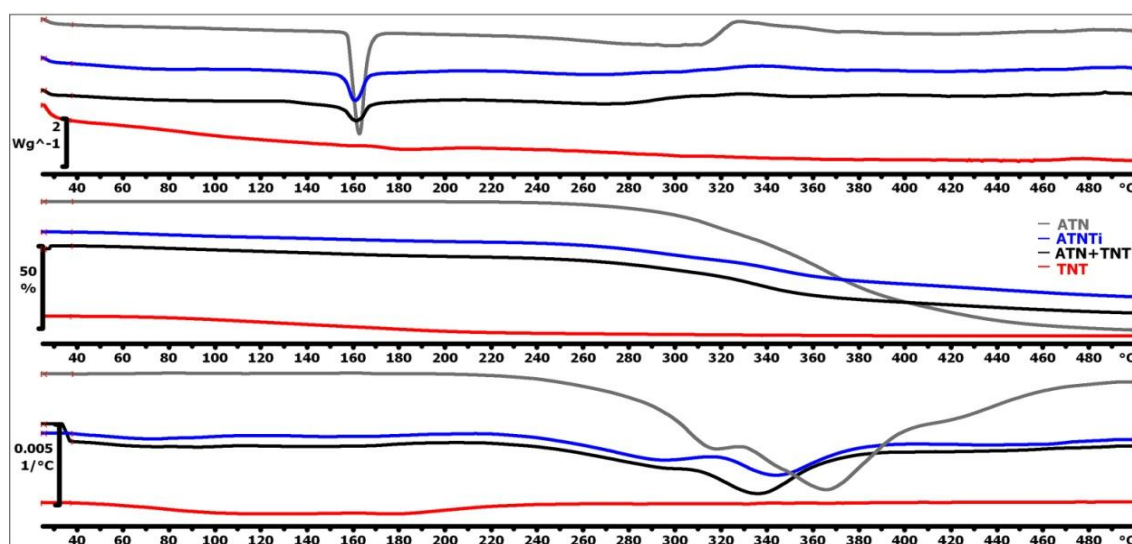


Figure 11. DSC, TG and DTG curves of ATN, ATNTi, ATN+TNT and TNT [96]

The evaluation of results of the last group of samples, HCT, HCT+TNT and HCTTi led to interesting findings. Based on the DSC curves it could be stated that the fusion of HCTTi and HCT+TNT slightly shifted to lower temperatures and showed decreased relative fusion enthalpy compared to HCT (Fig. 12, Table 7). While the shift of melting point was modest for HCT+TNT, it was definitely remarkable in the case of HCTTi with a shift of approx. 18 °C. As regards the decomposition process displayed in the DSC curves, it can be established that the characteristic exothermic event belonging to HCT barely appeared in the case of HCT+TNT and HCTTi. Nevertheless, it is easy to realize that the decomposition of HCTTi and HCT+TNT starts at higher temperatures as also confirmed by TG and DTG curves [96].

The evaluation of the evolved gases (Table 9) revealed that there is an ion fragment, $m/z=30$ appeared at 265 °C which is detectable only for HCTTi. This ion fragment probably represents N_2O derived from the sulfonamide group of HCT, indicating that the amino group plays important role in the composite formation, shifting the electron

structure of the molecule and therefore resulting in the detachment of the amino group at lower temperature [96].

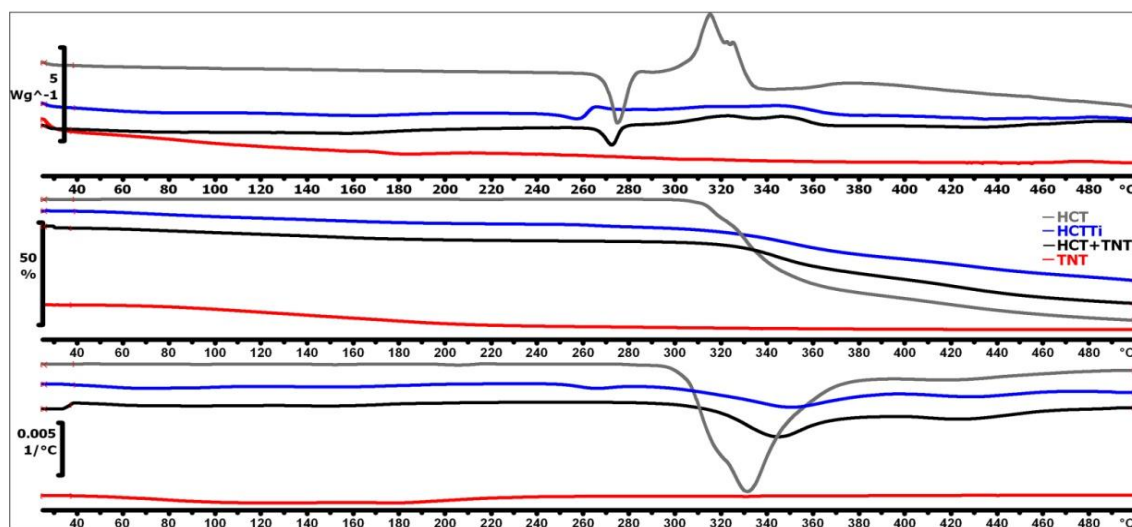


Figure 12. DSC, TG and DTG curves of HCT, HCTTi, HCT+TNT and TNT [96]

Table 9. Characteristics for the evolution of gases of HCT, HCTTi and HCT+TNT. T1, T2 and T3 are temperatures at the first, second and third peaks of the gas evolution [96]

	Mass (m/z)	16	17	18	30	44	48	50	64	66
HCT	Evolution range (°C)	330-451	333-455			303->500	295->500	304-401	295->500	304-402
	T1 (°C)	367	355			343	316	317	317	317
	Intensity of T1 (A)	1.38E-08	5.17E-08			6.94E-10	2.28E-09	1.59E-10	3.73E-09	1.72E-10
	T2 (°C)					428	324	234	326	326
	Intensity of T2 (A)					8.56E-10	2.10E-09	1.37E-10	3.37E-09	1.60E-10
	T3 (°C)						333	332	333	332
HCTTi	Intensity of T3 (A)						2.66E-09	1.72E-10	4.26E-09	1.99E-10
	Evolution range (°C)	331-405			247-293	238->500	257->500	256-475	250->500	256-474
	T1 (°C)	356			266	264	369	356	367	365
	Intensity of T1 (A)	2.50E-09			3.48E-09	4.85E-10	4.14E-10	5.79E-11	6.59E-10	3.26E-11
HCT+TNT	T2 (°C)					433	435		435	
	Intensity of T2 (A)					1.41E-09	4.06E-10		6.52E-10	
	Evolution range (°C)	317-396				333->500	276->500	285-476	288->500	
	T1 (°C)	344				428	358	349	363	
	Intensity of T1 (A)	3.03E-09				1.54E-09	4.34E-10	6.74E-11	6.80E-10	
	T2 (°C)					482	431		426	
	Intensity of T2 (A)					2.09E-09	5.84E-10		9.02E-10	

The resume of the thermoanalytical measurements shows a clear tendency: TNTs shift the fusion of an API to lower temperatures, which may be due to the decreased particle size and/or to the interactions of the API and TNTs. The decreased relative enthalpy of the peaks indicates that the composite formation puts the system into an energy minimum. The long-lasting decomposition is probably due to the TNT-API interactions on the interfacial surface, which may be observed both for physical mixtures and composites, but increased rate of extension was noticed in latter case. This may be due to the certainly

stronger interactions inside the composites, or can be explained by the location which results immediate decomposition of the surface-attached API, while the drug locked inside the nanotubes decomposes with a time lag. Overall, it can be established that DicNa and HCT are perfectly suitable to form stable API-TNT composites, while DiltHCl and ATN are less capable to form strong interactions with the TNTs [96].

5.1.4. FT-IR

FT-IR analysis of the materials was also performed to confirm the results and conception gained from the morphological and thermoanalytical measurements on TNT-API interactions within composites.

During the overview of the spectra of pure and incorporated APIs in various samples a common phenomenon was observed: a new intense peak appeared between $460\text{--}480\text{ cm}^{-1}$ overlapping with other signals in the $400\text{--}600\text{ cm}^{-1}$ region. This peak is assumed to reflect a general interaction between the electron system of the TNTs and the molecular skeleton of the APIs. Beside this common characteristic, results pointed out many drug specific spectral changes assigned to the incorporation. These are discussed below [96].

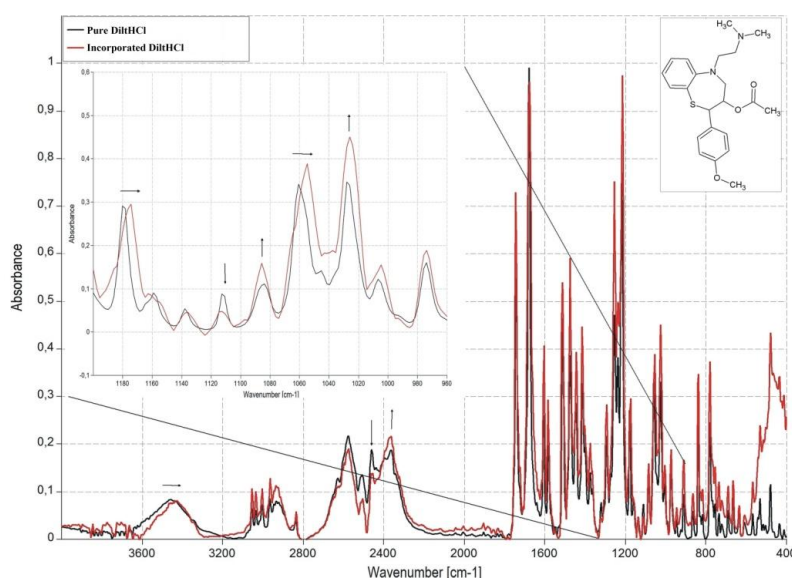


Figure 13. FT-IR spectra of pure and incorporated DiltHCl [96]

For better comparability, the spectra of pure and incorporated DiltHCl (Fig. 13) were normalized for the C=O stretching peak at 1680 cm^{-1} . The comparison of the spectra indicates that the amino groups of the molecule play the main role in the complexation process. The relative intensity decrease of the characteristic peaks belonging to N-H

stretching at 2579, 2509 and 2458 cm^{-1} , the relative increase and slight right shift of the peak from 2365 to 2360 cm^{-1} as well as the right shift of the peaks of C-N stretching at 1218, 1180, 1112 and 1060 cm^{-1} with approx. 5 cm^{-1} prove the main role of the ternary amino group in the stabilisation of the composite form. Moreover, the peak shifts in the 2800-3000 cm^{-1} region which indicate the torsion of the C-C molecular skeleton are also attributed to the hydrogen bonding of the nitrogen atoms. The other spectral differences e.g. the shoulder formation of the peak at 1730 cm^{-1} , the relative intensity decrease of peaks at 1610 and 1583 cm^{-1} (belonging to the =O group in the lactam ring), the shift of the peak from 1112 to 1085 cm^{-1} (C-S-C stretching) or the intensity increase of peaks at 1255, 1238 and 1220 cm^{-1} (Ar-O-Me vibration) show that beside the amino groups, the other hydrogen acceptor groups of the molecule also participate in the composite formation but in a less intensive way [96].

The spectra belonging to the pure and the incorporated DicNa (Fig. 14) were also normalized for the C=O stretching peak at 1575 cm^{-1} .

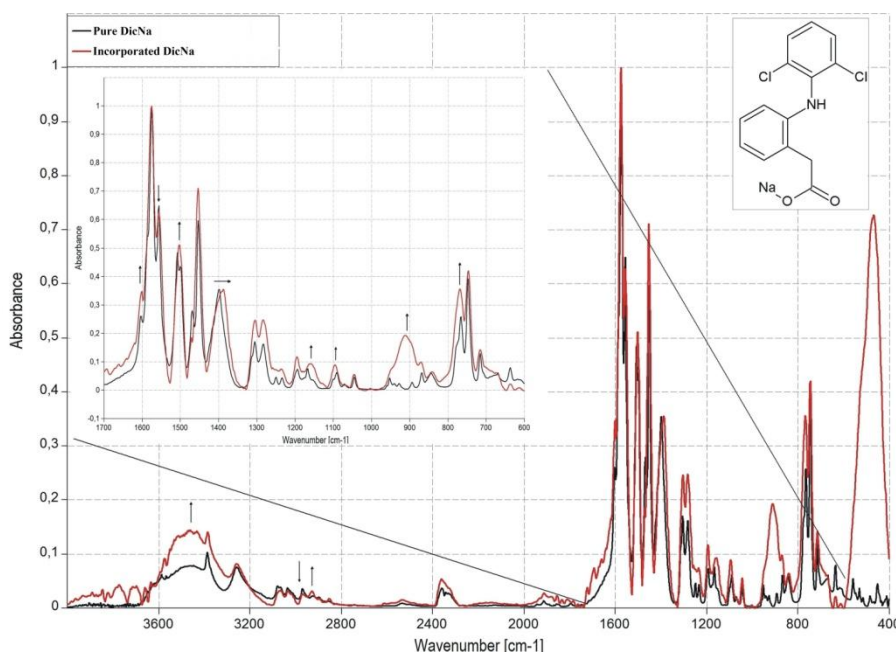


Figure 14. FT-IR spectra of pure and incorporated DicNa [96]

Based on the strong intensity increase of the O-H stretching peak at 3470 cm^{-1} and the shift of the C-O stretching peak from 1399 cm^{-1} to 1389 cm^{-1} the carboxyl group is highly involved in the complex formation as a hydrogen donor. Spectral changes attributed to the C-N vibrations such as the shift of the peaks from 3587 and 3447 to 3573 and 3433 cm^{-1}

respectively, and the signal widening at 2970 cm^{-1} and peak increments at 2928 , 2854 , 1300 and 1289 cm^{-1} confirm that the secondary amine group also acts as a hydrogen donor in the complex formation. Compared to the pure drug, the incorporated DicNa resulted in the appearance of some new peaks. A new medium intense peak was detected at 913 cm^{-1} which may indicate that the chloride groups are also involved into the conjugation as hydrogen acceptors. Furthermore, some weak signals appeared at 1725 and 1695 cm^{-1} suggesting that carbonyl oxygen also plays a minor role in the conjugation [96].

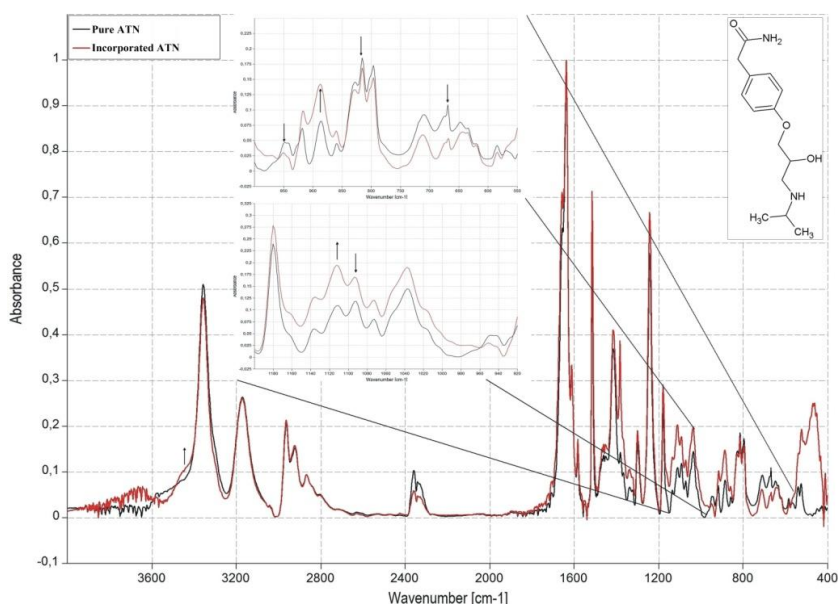


Figure 15. FT-IR spectra of pure and incorporated ATN [96]

As previously, the normalization of the pure and incorporated ATN spectra (Fig. 15) were done for the peak of the $\text{C}=\text{O}$ stretching at 1637 cm^{-1} . Based on the relative intensity decrease of the peak at 3357 cm^{-1} and the appearance of a peak shoulder at 3440 cm^{-1} , it can be established that the amide bond is an important hydrogen donor in the conjugation. The $\text{C}=\text{O}$ part of the amide bond is also involved in the composite formation as a hydrogen acceptor as indicated by the intensity increase at 1659 cm^{-1} and 1651 cm^{-1} . Besides, strong intensity increases were seen at 1385 cm^{-1} and 886 cm^{-1} which are assigned to the β -OH vibration of the secondary alcohol and C-O-C stretching of the ether bond, respectively. The peak shift detected from 1093 to 1112 cm^{-1} belongs to the secondary amino group while shifts in the $820\text{--}670\text{ cm}^{-1}$ region are related to the torsion of the molecular skeleton due to the conjugation process [96].

The spectra of pure and incorporated HCT (Fig. 16) were normalized for the S=O stretching peak at 1319 cm^{-1} . The compared spectra revealed that the NH association of the sulphonamide group plays a key role in the composite formation as a hydrogen donor. The direct spectra changes related to the NH part of the sulphonamide group are peak shifts from 3393 to 3362 cm^{-1} and from 3172 to 3168 cm^{-1} , while the indirect ones are shifts from 1453 to 1428 cm^{-1} and from 1403 to 1383 cm^{-1} belonging to the elongation of the C-S and S=O stretches (peak shifts at 1166 , 1153 and 1151 cm^{-1}). Based on the fact that only slight changes were seen in the 1190 - 1160 cm^{-1} region, the sulfone group is considered to take a minor part in the association. The multiple changes identified in the 910 - 520 cm^{-1} regions are mainly assigned to the modification in C-Cl stretching and the skeletal vibration of the benzothiazidine ring, and also indicate the slight participation of the NH groups in the association [96].

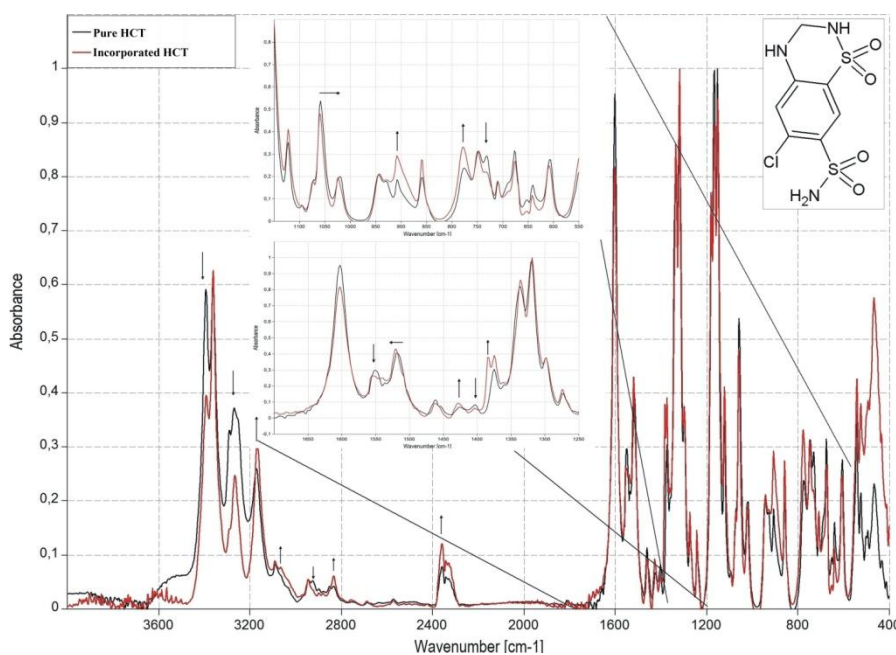


Figure 16. FT-IR spectra of pure and incorporated HCT [96]

The results of the FT-IR examination confirmed the thermoanalytical findings and also provided new essential information about the structure of the API-TNT composites. The assessment of the results pointed out that the strength of the association inside the composites is based on the hydrogen donor strength of the incorporated API. The hydrogen acceptor groups of the API play only a minor role in the association which can

be explained by the high quantity of OH groups (having poor hydrogen donating capacity) on the titanate surface (Fig. 17) [96].

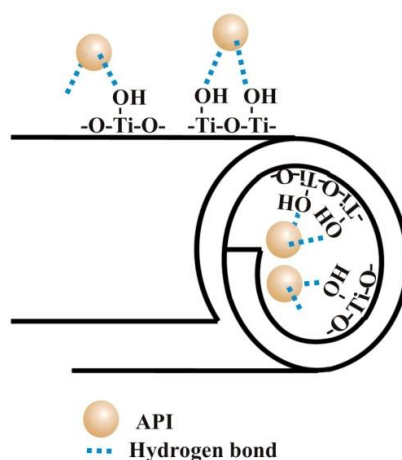


Figure 17. Association mechanism of APIs (DiltHCl, DicNa, ATN, HCT) with TNTs [96]

5.1.5. Powder rheology

Beside the knowledge on static properties of materials, information on their dynamic characteristics is also an essential criterion to provide optimized and robust formulations. The morphological and structural examinations provided promising results regarding to the static characteristics of the API-TNT composites, therefore investigation on the dynamic properties of these materials from the aspect of processability was also performed. In order to cover the whole tableting process, flowability, compressibility and compactibility of the materials were investigated.

Table 10. Powder rheological properties of TNTs, APIs and API-TNT composites [98]

Material	Flow time (sec)	Angle of repose (°)	Bulk density (g/cm ³)	Tapped density (g/cm ³)	Hausner Ratio	Compressibility Index (%)	Flowability (USP scale)
TNT	14,3	25,5	0,65	0,76	1,17	14,47	Good
DiltHCl	n.m*	-	0,45	0,59	1,31	23,73	Passable
DiltTi	16,5	28,2	0,51	0,64	1,25	20,31	Fair
DicNa	n.m.	-	0,48	0,73	1,52	34,25	very poor
DicTi	6,3	28,4	0,55	0,68	1,24	19,12	Fair
ATN	n.m.	-	0,3	0,48	1,6	37,5	very very poor
ATNTi	n.m.	-	0,38	0,49	1,29	22,45	Passable
HCT	n.m.	-	0,46	0,76	1,65	39,47	very very poor
HCTTi	n.m.	-	0,61	0,76	1,25	19,74	Fair

*not measurable

Based on the powder rheological properties (Table 10) it can be established that TNTs have good flowability and this affects the flow properties of the incorporated APIs in a

positive way; a great improvement of flowability is shown by DiltTi and DicTi compared to DiltHCl and DicNa, but the flowability improvement of ATNTi and HCTTi was less defined since these composites contain individual API crystals.. By evaluating the results as per the USP scale, it is clear that the flowability of the composites varies between those of the component materials. This can be explained by the fact that the APIs are located not only in the internal parts of the TNTs but on their surface as well. The rate of improvement may depend on the ratio of the surface coverage [98].

5.1.6. Compressibility and compactibility

Considering the powder rheological properties and crystal morphology of the APIs, their direct compression without excipients was an experimental challenge. The tableting experiments confirmed better compressibility and compactibility and easier operation with composites.

5.1.6.1. Energetic analysis

The energetic analysis affirmed the above experience and confirmed the benefit of the use of TNTs in every step of the tableting process. The evaluation of the conversion of MCW into ThCW is displayed in Fig. 18. The higher the slope, the smaller proportion of the applied MCW is lost on the initial particle rearrangement and converted into ThCW. According the R_1 values calculated from the slopes (Table 11), it can be concluded that pure APIs loose important energy on packaging and rearrangement of the particles due to their poor flowability and high adhesivity. The small R_1 values are in accordance with the powder rheological results (Table 10) and explain the hard accomplishment of the experiments. In contrast, the R_1 value belonging to TNTs indicates good flowability and favourable particle rearrangement properties. As expected, the composite products display results in between the TNTs and the pure APIs (Fig. 18). It is well visible that the composites show higher similarity with TNTs which confirms their relatively good flowability and packaging ability. Comparing the R_1 values of the composites, the following order can be set up: $HCTTi < ATNTi < DicTi < DiltTi$. This observation confirms the differences in the efficacy of the incorporation process presented in Section 5.1.1. In the case of DiltTi and DicTi, where the composite formation was ideal, the properties of TNTs dominate; the difference in their R_1 values may reflect to the different agglomeration mechanisms resulted by the different surface coverage of the TNTs with the API.

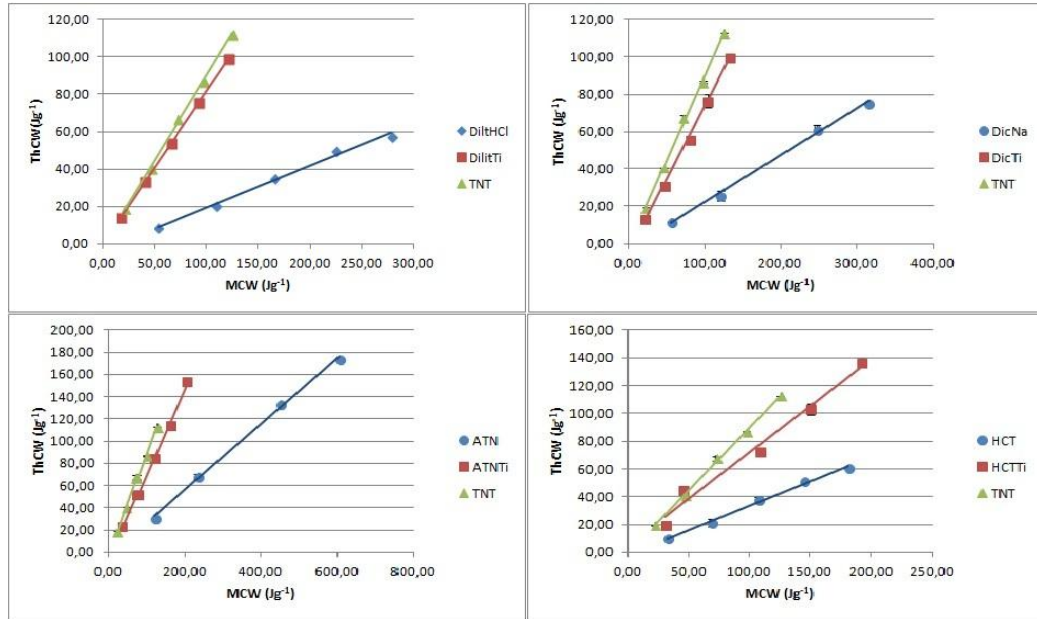


Figure 18. Evolution of ThCW with MCW of TNTs, APIs and API-TNT composites at 50, 100, 150, 200 and 250MP compression force [99]

As regards the ATNTi and HCTTi products, R_1 values represent the deficient composite formation; the smaller improvement seen for HCTTi may be related to the increase in surface free energy and adhesivity of the composite due to the nanotube coverage of the API [99].

Table 11. Energetic parameters of TNTs, APIs and API-TNT composites [99]

Material	R_1 (%)	R_2 (%)	R_3 (%)
TNT	88.65	16.32	82.87
DiltHCl	22.44	30.44	76.26
DiltTi	82.26	29.79	88.15
DicNa	25.52	29.52	59.16
DicTi	76.36	31.32	89.38
ATN	26.38	10.18	45.50
ATNTi	74.17	21.46	71.5
HCT	34.3	32.45	80.49
HCTTi	67.25	28.34	82.31

The TCW vs. ThCW plots (Fig. 19) were evaluated to calculate the energy dissipated on friction during the direct compression. In general, it could be established that the rate of friction is highly dependent on the surface free energy of the compressed material. In accordance with their high surface free energy, the compression of TNTs resulted in a low R_2 value (Table 11) indicating a massive energy loss on friction. In contrast, the lower surface free energy of the pure APIs resulted in modest energy loss on friction as displayed by the relatively high R_2 values. As for the composites, the

slope of curve varied by the surface coverage and consequential surface free energy of the products. In the case of DiltTi and DicTi where the TNTs are covered with drug nanocrystals, the characteristics of the incorporated APIs predominated resulting in parallel slopes of the composites and the pure APIs. In contrast, HCTTi showed similar friction properties as TNTs due to the nanotube coverage of the HCT crystals. The R_2 value of ATNTi was unexpected as it indicates decreased rate of friction compared to both the pure API and the TNTs, which may be due to weak hydrophilic interactions between the ATN and the TNTs which lend more hydrophobic characteristics to the composite [99].

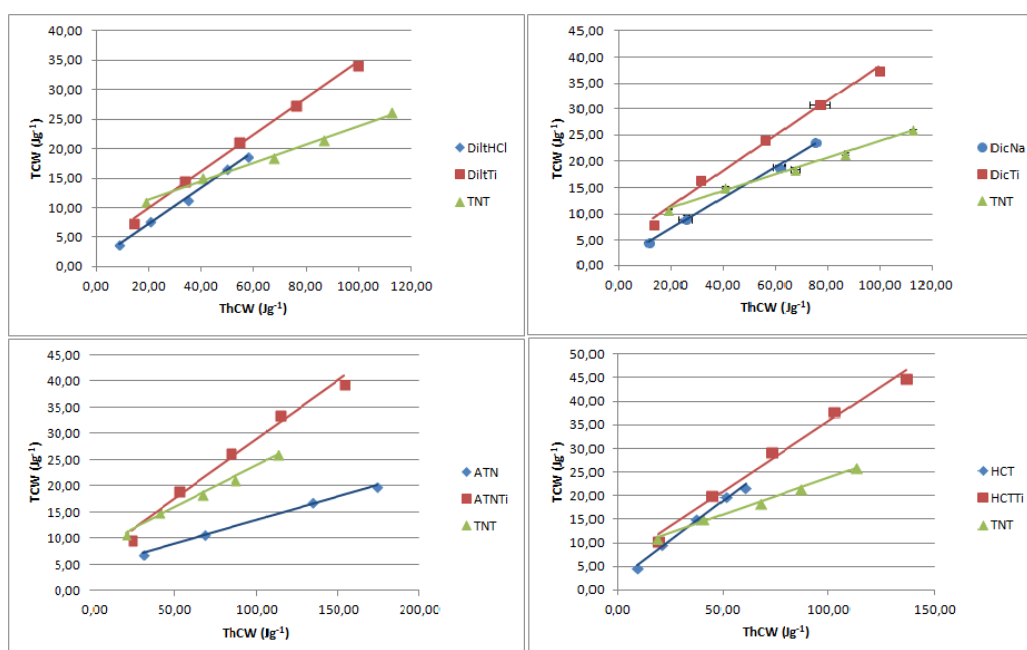


Figure 19. Evolution of TCW with ThCW of TNTs, APIs and API-TNT composites at 50, 100, 150, 200 and 250MP compression force [99]

The investigation of the conversion of the TCW into NCW (Fig. 20) allowed calculating the R_3 values (Table 11) which are indicatives of the deformation type. The higher the R_3 value, the more plastic is the deformation. When the R_3 values of all samples were compared, it became clear that the composite formation improves the plastic deformation of APIs over the elastic one. However, this positive effect depends on the efficacy of the incorporation. Accordingly, the most considerable improvement was seen in the case of the successfully incorporated DiltHCl and DicNa. The increase of R_3 value of DicNa is especially remarkable since the elastic recovery of the pure API was

so marked that the lamination of the tablets compressed above 150 MPa was clearly visible [99].

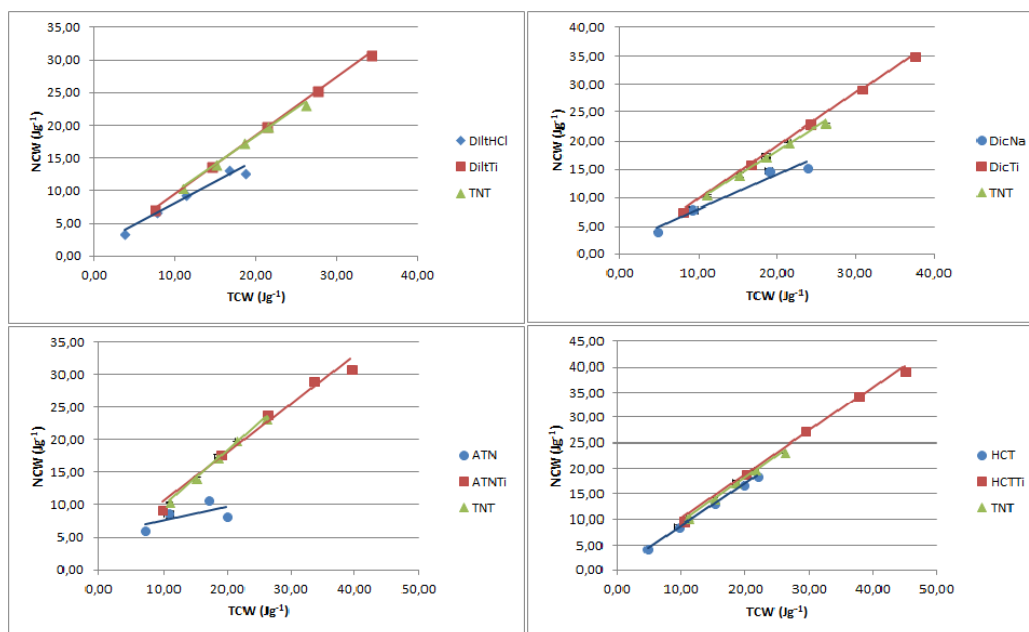


Figure 20. Evolution of NCW with TCW of TNTs, APIs and API-TNT composites at 50, 100, 150, 200 and 250MP compression force [99]

5.1.6.2. Post-compressional properties

The determination of the effect of compressibility and compactibility of materials on the post-compressional tablet properties can be used to estimate the efficacy of the tableting process. The post-compressional properties of tablets are summarized in Fig. 21, providing a complex image of the tablettability of the investigated materials.

Tablets prepared from pure APIs may be characterized by high (approx. 75–90 %) compaction ratio at low pressure which shows slight increase with the increment of compression pressure. Despite of the high compressibility, API tablets display very low tensile strengths indicating their poor compactibility. In contrast, TNTs show poor (approx. 55 %) compaction ratio at low compression force, but still result in tablets of high tensile strength in the whole compression force range and can be considered adequate for tableting. The results of the composite tablets need to be assessed one by one due to the unique characteristics. However, a clear tendency of improved tablettability can be established based on Fig. 21. It can be stated in general, that the composite tablets have higher tensile strength induced at lower compaction ratios

compared to the API tablets, which indicates that hard tablets can be produced with relatively high porosity, providing considerable benefits in drug release.

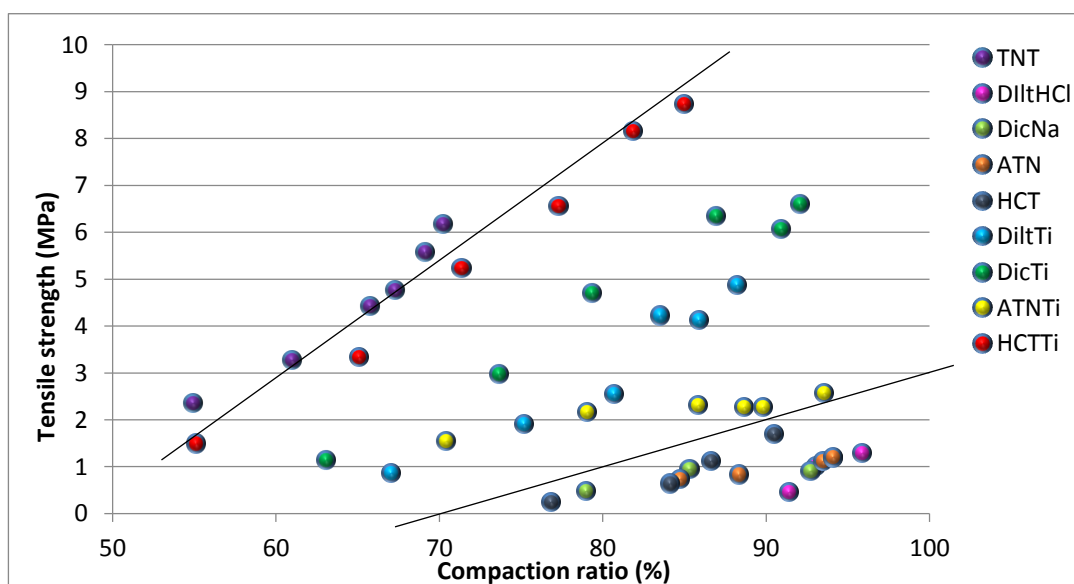


Figure 21. Evaluation of the tensile strength vs. the compaction ratio of the investigated materials compressed with 50, 100, 150, 200 and 250 MPa compression pressure [99]

Based on the results, DiltTi and DicTi tablets (where the APIs are well incorporated into the TNTs) have morefold higher tensile strengths compared to the DiltHCl and DicNa tablets at same compaction ratios. Furthermore, an immense improvement in tablettability could be recognized for DicNa/DicTi as the strong lamination of the DicNa tablets completely disappeared due to the composite formation. In case of the incompletely incorporated APIs (ATN and HCT), the properties of the composite tablets reflect a special mixture of the characteristics of the source materials. As regards the ATNTi, this resulted in relatively bad tablet properties which again prove the physical-mixture-like character of the ATNTi product. As concerns the HCTTi composite, the deficient incorporation of HCT induced more beneficial properties to the composite product than expected. The HCTTi tablets display not only far better tablet properties than all the other composites, but show even more favourable ones than the pure TNTs. This interesting phenomenon is probably due to the positive consonance of the reverse interaction between the HCT and the TNTs, and the good compactibility of both source materials [99].

5.2. Powder mixtures: APIs, API-TNT composites with excipients

The thorough investigation of the raw materials including their tablettability (flowing properties, compressibility, compactibility) already gave an idea about the potential benefit TNTs can provide as drug carriers in the process of direct compression. Since this benefit seemed promising in theoretical circumstances, the series of examinations was continued under realistic conditions. The aim of the tableting of powder mixtures (APIs, API-TNT composites with excipients) was to reveal whether the positive effect of TNTs on tableting remains notable or disappears by the use of excipients.

5.2.1. Compressibility and compactibility

The compressibility characteristics and the deformation mechanism of the powder mixtures (Table 2) were determined by applying the Kawakita-Lüdde and the Walker statistical models. These models are popular because they are easy to use and provide reliable results at once. Also, they are commonly used together as they complement well one another. The calculated constant values are summarized in Table 12.

Table 12. Parameters calculated from Kawakita and Walker plots [98]

Tablet	<i>A</i>	<i>1/b</i>	<i>L</i>	<i>W</i>
DiltHCl	0.68	8.03	7.9	11.59
DiltTi	0.62	18.63	5.93	16.49
DicNa	0.67	6.38	9.85	8.72
DicTi	0.68	13.53	6.64	14.73
ATN	0.64	5.94	13.56	4.04
ATNTi	0.65	17.61	8.47	9.43
HCT	0.61	14.32	12.89	7.01
HCTTi	0.68	6.04	17.76	2.49

The constant *a* values (Table 12), which demonstrate the rearrangement of the particles, are very similar for all the samples. Despite the fact that the results obtained for the raw materials presumed lower constant *a* values for the API-TNT tablet compositions, no considerable differences occurred neither within the API tablet compositions nor between the API and the related API-TNT tablet compositions. This allows concluding that the excipients were appropriately selected and could compensate the poor flow properties of APIs during packaging. However, it is notable that API-TNT powder mixtures contain proportionally less excipient than those of the APIs which means that TNTs could replace the function of the excipients [99].

In contrast, the constant *1/b* values of the API and API-TNT tablet compositions (Table 12), which correlate with the cohesiveness, display decided differences. Powders with

higher I/b values need more energy investment to reduce the volume of the powder bed to the half of the original in the rearrangement phase. The high I/b values of API-TNT tablet compositions are in accordance with the smaller compaction ratios of the API-TNT composites (Fig. 21). The low I/b values of the API tablet compositions is due to the fast collapse of the powder bed in the die resulting limited compressibility as it was observed for the pure API powders (Fig. 21). It is clear from the results that the behaviour of the HCT and HCTTi tablet compositions is exceptional since the HCT tablet composition has a quite high I/b value, while the HCTTi tablet composition displays an unexpectedly low I/b value. This phenomenon is probably due to the inverse composite formation mechanism which results in higher surface free energy and adhesivity of HCTTi compared to the pure HCT, which is resulted in decreased compactibility [98].

The values of coefficient L (Table 12) were lower for the API-TNT tablet compositions, indicating higher volume reduction of the composite containing compositions at a certain pressure in the deformation phase compared to the API tablet compositions. The opposite behaviour of the HCT/HCTTi tablet compositions appeared here as well due to the previously mentioned structural properties of the composite [98].

The coefficient W value correlates with the irreversible compressibility of the powders. Accordingly, the higher W values of the API-TNT tablet compositions reflect to their plastic deformation while the lower values displayed by the API tablet compositions refer to their high elastic recovery resulting in an exceeded densification maximum. These findings are in accordance with the results obtained for the deformation mechanism of the raw materials (Fig. 20). Here again, the behaviour of the HCT/HCTTi tablet powder mixtures occurred to be just the opposite of that of the other API/API-TNT tablet compositions for the already mentioned reason [98].

In general, it can be concluded that the results of the powder mixtures correlate well with the observations of the energetic analysis of the raw materials. The only exception is the case of HCT/HCTTi, where the raw materials indicate the positive effect of the composite formation, while this effect seems unfavourable in the powder mixtures.

Overall, it can be established that the incorporation of drugs into TNTs has a positive effect on the tablettability and therefore TNTs can be considered as a multifunctional excipient in tablet production. However, it is important to note that an unsuccessful composite formation can even lead to a worse tablettability profile than expected from the pure API itself [98].

5.2.2. Tablet properties

The tablet properties provide substantial information about the adequacy of the formulation procedure as well as about the therapeutic utility of the tablet. In the present study the tablet examination served to confirm the results of the Kawakita-Lüdde and Walker models and at the same time to give an explanation to the exceptional tableting results of the HCTTi tablet powder mixture. In addition, the measurements aimed to get an overall idea about the effects and potential pharmaceutical benefits of the use of hydrothermally synthesized TNTs in the manufacturing of tablets with direct compression.

5.2.2.1. Tablet density

The apparent densities of the tablets, which were calculated from the geometrical parameters measured right after the compression and one week later, are displayed in Table 13.

Table 13. Apparent density of the API and API-TNT tablets determined right after the preparation and one week later [98]

Pressing force(kN)	Apparent density (g/cm ³) ± SD							
	0 h (left columns); 168 h (right columns)							
	DiltHCl		DicNa		ATN		HCT	
5.0	1.09 ± 0.01	1.06 ± 0.01	1.16 ± 0.01	1.16 ± 0.01	1.11 ± 0.01	1.25 ± 0.01	1.03 ± 0.01	1.28 ± 0.01
7.5	1.18 ± 0.01	1.15 ± 0.01	1.23 ± 0.02	1.26 ± 0.02	1.04 ± 0.01	1.28 ± 0.01	1.07 ± 0.01	1.33 ± 0.01
10.0	1.25 ± 0.01	1.23 ± 0.01	1.27 ± 0.01	1.32 ± 0.02	1.01 ± 0.01	1.28 ± 0.01	1.09 ± 0.03	1.39 ± 0.01
12.5	1.29 ± 0.01	1.27 ± 0.01	1.30 ± 0.01	1.35 ± 0.02	0.93 ± 0.00	1.30 ± 0.01	1.11 ± 0.00	1.40 ± 0.00
15.0	1.30 ± 0.07	1.28 ± 0.08	1.34 ± 0.01	1.40 ± 0.01	0.92 ± 0.01	1.32 ± 0.01	1.12 ± 0.00	1.41 ± 0.00
	DiltTi		DicTi		ATNTi		HCTTi	
5.0	1.23 ± 0.01	1.23 ± 0.00	1.16 ± 0.00	1.16 ± 0.01	1.15 ± 0.01	1.31 ± 0.01	1.17 ± 0.00	1.39 ± 0.01
7.5	1.30 ± 0.00	1.30 ± 0.00	1.23 ± 0.01	1.23 ± 0.02	1.20 ± 0.01	1.37 ± 0.00	1.20 ± 0.01	1.42 ± 0.00
10.0	1.35 ± 0.02	1.35 ± 0.01	1.32 ± 0.00	1.32 ± 0.00	1.23 ± 0.01	1.40 ± 0.01	1.26 ± 0.00	1.48 ± 0.01
12.5	1.40 ± 0.01	1.39 ± 0.00	1.36 ± 0.01	1.35 ± 0.02	1.24 ± 0.01	1.42 ± 0.01	1.31 ± 0.00	1.48 ± 0.01
15.0	1.42 ± 0.00	1.40 ± 0.00	1.42 ± 0.00	1.40 ± 0.04	1.25 ± 0.02	1.43 ± 0.01	1.37 ± 0.00	1.52 ± 0.00

As expected, the tablets showed increased density with the increase of the compression force. The only exception was noticed for the ATN tablets during the 0 h measurements, where the density decreased with the increase of the compression force. The observed change in the density indicates the strong elasticity of the ATN resulting in an increasing elastic recovery with the increasing compression pressure, which corresponds with the

low coefficient W value of the ATN tablet composition (Table 12). The previously established positive effect of TNTs on the deformation mechanism is confirmed by the fact that no such phenomenon was identified for the ATNTi tablets. API-TNT tablets have higher apparent densities at all investigated compression pressures than the corresponding API containing tablets indicating that the presence of TNTs generally increases the apparent density of the produced tablets. However, the rate of this effect varies with the properties of the incorporated drug; in case of DicNa/DicTi tablets, where the incorporated API has good rearrangement and compressibility (Table 12), the increment in the apparent density appears only at higher compression forces. When comparing the apparent density changes in time, it turned out that the apparent density of the DicNa, ATN and HCT tablets increases, while the density of the DiltHCl tablets decreases during the one-week storage. The increase in density is attributed to the consolidating bonding forces, while the decrease in density is assigned to the release of the stored stress by the tablet by increasing its volume. As regards the API-TNT tablets, no remarkable density changes were detectable for the DiltTi and DicTi tablets at any compression forces confirming the previously detected plastic deformation of these powder mixtures. However, the ATNTi and HCTTi tablets showed increased apparent density after one-week storage at all compression forces. Based on the similar density changes of ATN and HCT tablets, these results are certainly due to the incomplete composite formation [98].

5.2.2.2. Breaking force and tensile strength

The breaking force and the tensile strength are important indicators of the tablet quality and therefore reflect to the suitability of the tablet composition and the formulation setups.

As displayed in Table 14, the breaking strength increases with the compression pressure for every tablet compositions, but the increment is greater for the API-TNT tablets than for the API tablets. Furthermore, the breaking strengths of the API-TNT tablets are much superior to those of the API tablets at all compression forces. These results are in agreement with the compaction properties of the powder mixtures (Table 12) and the raw materials as well (Fig. 21). According to Table 14, the less influence of the composite formation on the breaking strength was for DicNa and DicTi tablets. This observation is consonant with the results of the apparent density measurements. The comparison of the four APIs revealed that HCT (and therefore HCTTi) tablets have the biggest breaking

strengths at each compression force which correlates with their high apparent density values (Table 13) as well as with the observations of the post-compressional properties of the raw materials (Fig. 21) [98].

Table 14. Breaking and tensile strength of the API and API-TNT tablets [98]

Pressing force (kN)	Breaking strength (N) \pm SD			
	DiltHCl	DicNa	ATN	HCT
5.0	24.9 \pm 1.1	42.9 \pm 2.64	79.5 \pm 2.90	87.0 \pm 4.20
7.5	53.0 \pm 3.63	58.1 \pm 3.68	82.4 \pm 2.08	112.0 \pm 3.84
10.0	66.2 \pm 4.47	81.2 \pm 4.58	89.6 \pm 1.60	149.0 \pm 4.81
12.5	104.0 \pm 4.53	98.1 \pm 3.91	101.0 \pm 4.27	153.0 \pm 3.40
15.0	124.0 \pm 3.19	125.0 \pm 3.00	102.0 \pm 3.08	160.0 \pm 4.00
	DiltTi	DicTi	ATNTi	HCTTi
5.0	69.0 \pm 1.79	46.0 \pm 3.04	102.0 \pm 4.56	127.0 \pm 3.16
7.5	96.0 \pm 2.37	66.0 \pm 2.80	121.0 \pm 1.97	148.0 \pm 3.64
10.0	122.0 \pm 4.86	99.0 \pm 3.63	138.0 \pm 2.77	190.0 \pm 3.10
12.5	142.0 \pm 2.66	120.0 \pm 3.30	141.0 \pm 2.19	191.0 \pm 3.50
15.0	156.0 \pm 2.86	153.0 \pm 3.05	149.0 \pm 4.34	222.0 \pm 2.72
Pressing force (kN)	Tensile strength (N) \pm SD			
	DiltHCl	DicNa	ATN	HCT
5.0	0.47 \pm 0.02	0.85 \pm 0.05	1.68 \pm 0.06	1.63 \pm 0.08
7.5	1.09 \pm 0.06	1.21 \pm 0.08	1.75 \pm 0.04	2.18 \pm 0.07
10.0	1.60 \pm 3.68	1.74 \pm 0.07	1.99 \pm 0.04	2.92 \pm 0.20
12.5	2.35 \pm 0.08	2.17 \pm 0.08	2.02 \pm 0.09	3.10 \pm 0.06
15.0	2.83 \pm 0.10	2.73 \pm 0.07	2.13 \pm 0.08	3.22 \pm 0.10
	DiltTi	DicTi	ATNTi	HCTTi
5.0	1.42 \pm 0.04	0.93 \pm 0.05	1.99 \pm 0.09	2.65 \pm 0.07
7.5	2.08 \pm 0.05	1.44 \pm 0.05	2.48 \pm 0.05	3.14 \pm 0.07
10.0	2.83 \pm 0.09	2.27 \pm 0.08	2.88 \pm 0.05	4.13 \pm 0.07
12.5	3.37 \pm 0.06	2.83 \pm 0.07	3.00 \pm 0.05	4.32 \pm 0.08
15.0	3.79 \pm 0.05	3.80 \pm 0.06	3.24 \pm 0.09	5.14 \pm 0.06

5.2.2.3. Disintegration and drug dissolution

The disintegration time of a tablet is essential regarding the drug dissolution. For this reason and in order to define the effect of the composite formation on the disintegration, the disintegration time of the API and API-TNT tablets has been determined. The results are summarized in Table 15.

Supporting the expectations, the disintegration time appeared to be proportional with the compression pressure in all cases, and the disintegration time of the API-TNT tablets is longer than that of the corresponding API tablets which correlates with their greater hardness (Table 14). Nevertheless, despite their high hardness and apparent density, the HCT and HCTTi tablets disintegrate very quickly and with quite similar disintegration

times. Furthermore, their disintegration shows less dependence on the compression pressure when compared to other tablet compositions.

Table 15. Disintegration time of the API and API-TNT tablets [98]

Pressing force (kN)	Disintegration time (min) \pm SD			
	DiltHCl	DicNa	ATN	HCT
5.0	0.16 \pm 0.02	0.20 \pm 0.01	1.05 \pm 0.09	0.12 \pm 0.02
7.5	0.41 \pm 0.17	0.41 \pm 0.05	1.56 \pm 0.28	0.18 \pm 0.03
10.0	8.28 \pm 0.68	1.05 \pm 0.13	3.33 \pm 0.33	0.23 \pm 0.06
12.5	11.07 \pm 1.34	1.58 \pm 0.19	5.40 \pm 0.48	0.23 \pm 0.06
15.0	18.13 \pm 0.52	4.23 \pm 0.05	6.26 \pm 0.18	0.28 \pm 0.03
Pressing force (kN)	Disintegration time (min) \pm SD			
	DiltTi	DicTi	ATNTi	HCTTi
5.0	0.52 \pm 0.03	1.34 \pm 0.09	4.95 \pm 0.35	0.31 \pm 0.06
7.5	2.44 \pm 0.29	2.13 \pm 0.05	9.56 \pm 0.17	0.48 \pm 0.16
10.0	9.54 \pm 0.49	3.21 \pm 0.41	13.40 \pm 0.37	1.18 \pm 0.13
12.5	15.49 \pm 0.27	4.26 \pm 0.65	15.30 \pm 0.46	1.43 \pm 0.07
15.0	18.46 \pm 0.52	5.27 \pm 0.37	18.62 \pm 0.43	3.19 \pm 0.30

The explanation to this phenomenon was found in the SEM pictures of the broken surfaced tablets (Fig. 22) which pointed out fragmentations of the HCT particles (marked with yellow arrows). These fragmentations may provoke the before observed irregularly high densification of both the HCT and HCTTi tablet compositions and are responsible for the fast disintegration process as well. The microfractures let the water penetrate in the HCT particles and disrupt them by the fractures. The released energy speeds up the disintegration process [98].

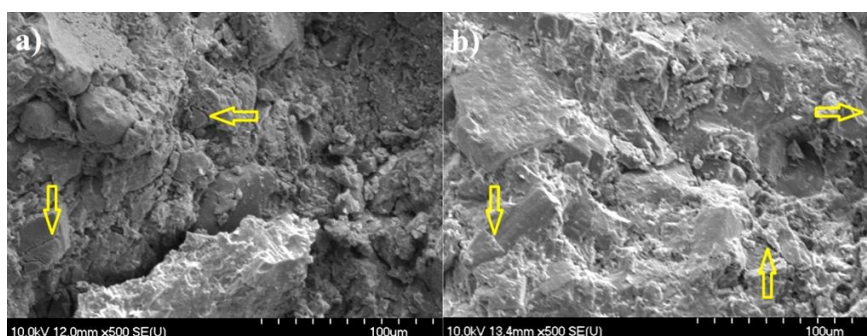


Figure 22. SEM images of the breaking surface of HCTTi 5kN (a) and 15kN tablets (b) [98]

The dissolution tests were performed with two important goals: to reflect to the tablet properties and to reveal the influences of the composite formation on the solubility and dissolution profile of the APIs.

The results of the dissolution tests in pH 6.8 phosphate buffer are displayed in Fig. 23. Regarding to the expectations no considerable change was observed in the dissolution profiles of the well soluble DiltHCl/DiltTi or ATN/ATNTi tablets, except of the decreased dissolution speed with the increasing compression pressure or resulted by the bigger density of the API-TNT tablets.

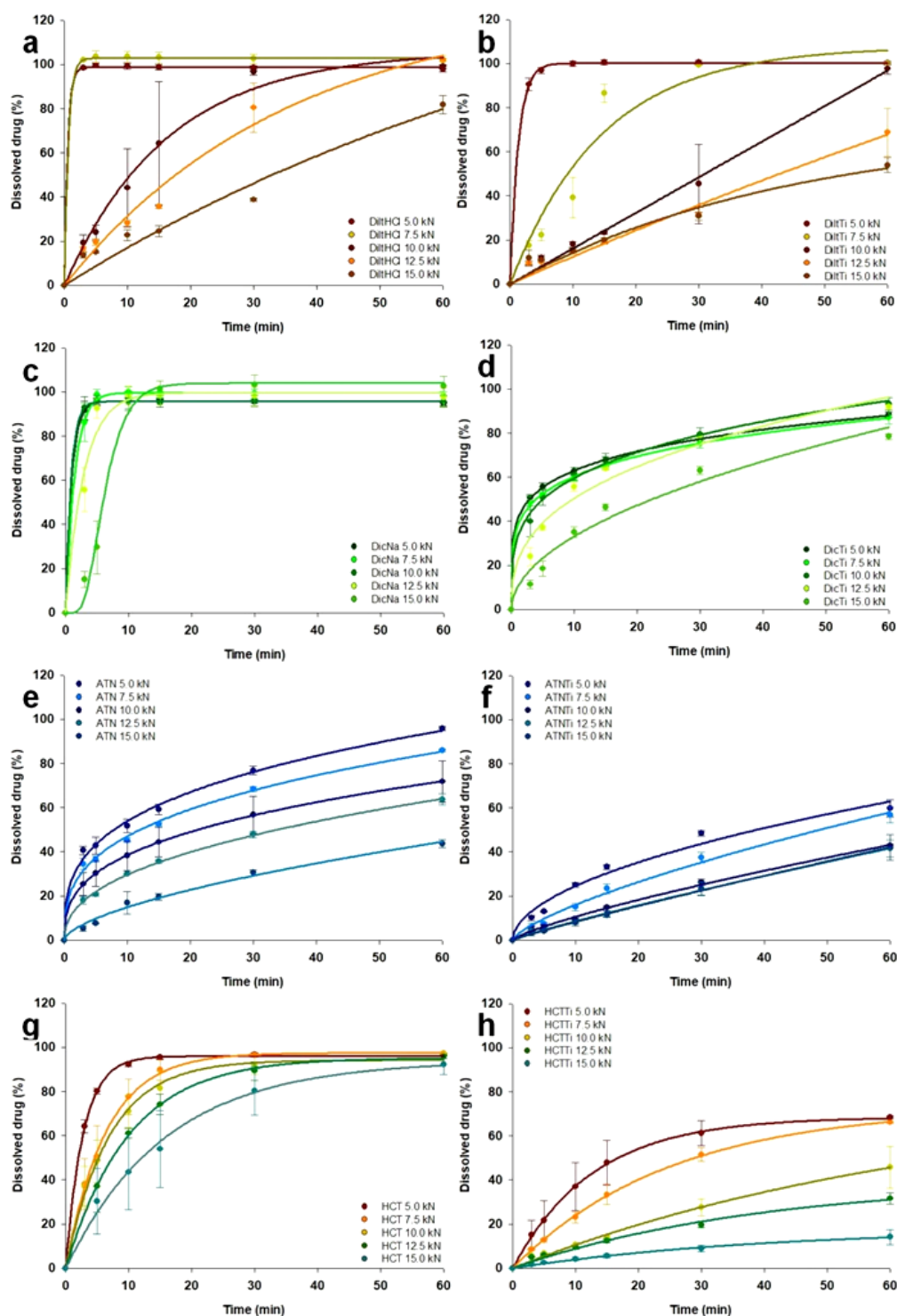


Figure 23. Dissolution study of API and API-TNT tablets in phosphate buffer [98]

The dissolution profiles of the HCT/HCTTi tablets were also highly similar, which may be due to the incomplete incorporation and non-considerable particle size decrease of HCT. In contrast, considerable changes in drug release profile were noted for the DicNa/DicTi tablets, due to the strong drug-carrier interactions. The dissolution from DicNa tablets follows a first order dissolution profile as per Noyes-Whitney equation, while DicTi tablets shows prolonged drug release kinetics according to Korsmeyer-Peppas equation. In this case the TNTs act as a standalone matrix system, which may be utilized as modified-release drug delivery system. Furthermore, in contrast with the other investigated API/API-TNT tablets, an improved dissolution rate was observed from DicTi tablets compared to DicNa tablets in artificial gastric juice (Fig. 24). Since DicNa is poorly soluble under gastric conditions, this phenomenon may be due to the particle size decrease of DicNa which doubled the rate and the amount of the dissolved API. This observation is essential since it proves the solubility increasing capacity of TNTs [96], [98].

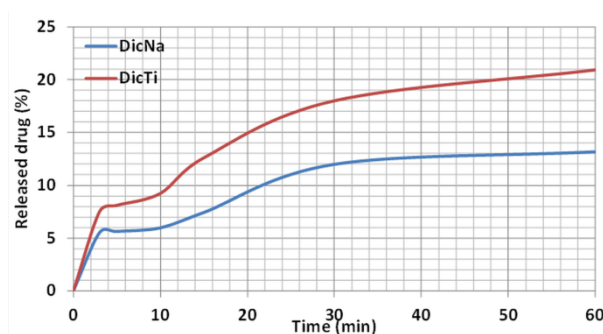


Figure 24. Dissolution from DicNa and DicTi 5kN tablets in artificial gastric juice

It can be generally stated that the first phase of dissolution is driven by the disintegration, while the slower drug dissolution in the further phases is attributed to the interactions inside the composites which retain the incorporated APIs from the quick release to different extents [98].

Overall, the dissolution studies allowed concluding that the presence of TNTs increases the tablet strength and results prolonged drug release without reference to the success of the composite formation process. However, in case of successful drug incorporation and adequate strength of interactions inside the composite, TNTs can modify the kinetics of the drug dissolution., or in the case of an ideal composite formation process, TNTs are able to improve the solubility of the incorporated drug by decreasing its particle size [96], [98].

6. CONCLUSIONS

The main consequences of the research may be summarized as follows.

The measurements revealed that only two (DiltHCl and DicNa) out of the four investigated APIs were successfully incorporated into the TNTs. It indicates that the applied composite formation method (Section 4.1.1.) is only conditionally suitable since its efficacy highly depends on the physicochemical properties of the drug to be incorporated. Therefore, further optimization of the method may be required before use.

We have determined that API-TNT interactions are principally based on hydrogen bonds and the strength of the association depends on the hydrogen donor strength of the incorporated API. The hydrogen acceptor groups of the API play only secondary role in the association due to the high quantity, but poor hydrogen donating capacity of OH groups on the surface of titanate nanotubes. Accordingly, the strongest association was seen for DicTi and HCTTi among the investigated composites.

The API-TNT association and the particle size reduction resulted decreased fusion temperature and enthalpy, and modified and elongated decomposition of the APIs. The change in the thermal behaviour was affected by the strength of interactions, therefore the most important differences were observed for the DicNa/DicTi and HCT/HCTTi samples.

The image analysis and surface energy measurements revealed that the API may be located both in the inner parts and on the surface of the TNTs. The resulted decrease of the surface free energy may lead to improved flow and packaging characteristics.

The good tableting properties of the TNTs highly improved the tablettability of the incorporated APIs due to improved flowability, packaging, extended range of compressibility and better compactibility. However, these effects showed considerable dependence on the efficacy of the incorporation and therefore the best results were recorded for DiltHCl and DicNa. As regards the post-compressional tablet properties, the composite formation extremely improved the tablet strength, increased the density and therefore slowed down the disintegration and prolonged the drug dissolution. The positive effect of TNTs on the tablet properties was far less influenced by the success of the incorporation than observed for other parameters.

Nevertheless, API-TNT interactions may affect the drug release from the composite product by acting as a matrix and retaining the release of the API over certain strength of interactions, as was observed in the case of DicNa. However, the decreased particle size may lead to better solubility of poorly soluble drugs, especially if the release is not disintegration-driven, as was observed in the case of 5kN DicTi tablets in artificial gastric juice.

Finally, this research proved that drug loaded TNTs can successfully and easily be formulated into tablets with direct compression method, since they are capable to improve every step of the tableting cycle and lead to favourable tablet properties even when used in small quantity and when compared to other excipients. Accordingly, TNTs have the potential to replace and over fulfil one or more excipients in a tablet composition and therefore can improve and simplify the production. Furthermore, if the API is correctly incorporated in the TNTs, these carriers can improve the drug solubility which may be promising for pharma-industry since TNTs can become alternatives of available nanocarriers with fundamental manufacturing problems such as dendrimers, liposomes, etc. In addition, by carrying nanosized drugs, TNTs may overcome the autoaggregation induced formulation difficulties of nanocrystalline APIs.

7. REFERENCES

- [1] Y. Jia, Y. Ma, Y. Lin, J. Tang, W. Shi, and W. He, "In-situ growth of hierarchical NiCo₂S₄/MoS₂ nanotube arrays with excellent electrochemical performance," *Electrochim. Acta*, vol. 289, pp. 39–46, Nov. 2018.
- [2] W. Zhu, Y. Liu, A. Yi, M. Zhu, W. Li, and N. Fu, "Facile fabrication of open-ended TiO₂ nanotube arrays with large area for efficient dye-sensitized solar cells," *Electrochim. Acta*, vol. 299, pp. 339–345, Mar. 2019.
- [3] Y. Zhou, X. Zhou, C. Ge, W. Zhou, Y. Zhu, and B. Xu, "Branched carbon nanotube/carbon nanofiber composite for supercapacitor electrodes," *Mater. Lett.*, vol. 246, pp. 174–177, Jul. 2019.
- [4] W.-L. Xu, M.-S. Niu, X.-Y. Yang, J. Xiao, H.-C. Yuan, C. Xiong, and X.-T. Hao, "Carbon nanotubes as the effective charge transport pathways for planar perovskite photodetector," *Org. Electron.*, vol. 59, pp. 156–163, Aug. 2018.
- [5] M. A. Dobrovolskaia, "Pre-clinical immunotoxicity studies of nanotechnology-formulated drugs: Challenges, considerations and strategy.," *J. Control. Release*, vol. 220, no. Pt B, pp. 571–83, Dec. 2015.
- [6] M. Kulkarni, A. Mazare, E. Gongadze, S. Perutkova, V. Kralj-Iglić, I. Milošević, P. Schmuki, A. Iglič, and M. Mozetič, "Titanium nanostructures for biomedical applications," *Nanotechnology*, vol. 26, no. JANUARY, p. 62002 (1-18), 2015.
- [7] S. Minagar, C. C. Berndt, J. Wang, E. Ivanova, and C. Wen, "Acta Biomaterialia

A review of the application of anodization for the fabrication of nanotubes on metal implant surfaces,” *Acta Biomater.*, vol. 8, no. 8, pp. 2875–2888, 2012.

[8] D. Regonini, C. R. Bowen, a. Jaroenworarluck, and R. Stevens, “A review of growth mechanism, structure and crystallinity of anodized TiO₂ nanotubes,” *Mater. Sci. Eng. R Reports*, vol. 74, no. 12, pp. 377–406, 2013.

[9] A. W. Tan, B. Pingguan-Murphy, R. Ahmad, and S. A. Akbar, “Review of titania nanotubes: Fabrication and cellular response,” *Ceram. Int.*, vol. 38, no. 6, pp. 4421–4435, Aug. 2012.

[10] T. Brunatova, D. Popelkova, W. Wan, P. Oleynikov, S. Danis, X. Zou, and R. Kuzel, “Study of titanate nanotubes by X-ray and electron diffraction and electron microscopy,” *Mater. Charact.*, vol. 87, pp. 166–171, 2014.

[11] L. Fernández-Werner, F. Pignanelli, B. Montenegro, M. Romero, H. Pardo, R. Faccio, and Á. W. Mombrú, “Characterization of titanate nanotubes for energy applications,” *J. Energy Storage*, vol. 12, pp. 66–77, 2017.

[12] S. Muniyappan, T. Solaiyammal, K. Sudhakar, A. Karthigeyan, and P. Murugakoothan, “Conventional hydrothermal synthesis of titanate nanotubes: Systematic discussions on structural, optical, thermal and morphological properties,” *Mod. Electron. Mater.*, vol. 3, no. 4, pp. 174–178, Dec. 2017.

[13] D. Xu, J. Li, Y. Yu, and J. Li, “From titanates to TiO₂ nanostructures: Controllable synthesis, growth mechanism, and applications,” *Sci. China Chem.*, vol. 55, no. 11, pp. 2334–2345, 2012.

[14] K. R. Zhu, Y. Yuan, M. S. Zhang, J. M. Hong, Y. Deng, and Z. Yin, “Structural transformation from NaHTi₃O₇ nanotube to Na₂Ti₆O₁₃ nanorod,” *Solid State Commun.*, vol. 144, no. 10–11, pp. 450–453, Dec. 2007.

[15] R. Camposeco, S. Castillo, J. Navarrete, and R. Gomez, “Synthesis, characterization and photocatalytic activity of TiO₂ nanostructures: Nanotubes, nanofibers, nanowires and nanoparticles,” *Catal. Today*, vol. 266, pp. 90–101, Oct. 2015.

[16] N. Liu, X. Chen, J. Zhang, and J. W. Schwank, “A review on TiO₂-based nanotubes synthesized via hydrothermal method: Formation mechanism, structure modification, and photocatalytic applications,” *Catal. Today*, vol. 225, pp. 34–51, 2014.

[17] A. Gajović, I. Frišćić, M. Plodinec, and D. Iveković, “High temperature Raman spectroscopy of titanate nanotubes,” *J. Mol. Struct.*, vol. 924–926, pp. 183–191, Apr. 2009.

[18] M. Á. López Zavala, S. A. Lozano Morales, and M. Ávila-Santos, “Synthesis of stable TiO₂ nanotubes: effect of hydrothermal treatment, acid washing and annealing temperature,” *Heliyon*, vol. 3, no. 11, p. e00456, Nov. 2017.

[19] F. Sallem, R. Chassagnon, A. Megriche, M. El Maaoui, and N. Millot, “Effect of mechanical stirring and temperature on dynamic hydrothermal synthesis of titanate nanotubes,” *J. Alloys Compd.*, vol. 722, no. October, pp. 785–796, 2017.

[20] B. Wang, D. Xue, Y. Shi, and F. Xue, “Titania 1D nanostructured materials: synthesis, properties and applications,” *Nanorods, Nanotub. Nanomater. Res. Prog.*, pp. 163–201, 2008.

[21] J. Yu, G. Wang, B. Cheng, and M. Zhou, “Effects of hydrothermal temperature and time on the photocatalytic activity and microstructures of bimodal mesoporous TiO₂ powders,” *Appl. Catal. B Environ.*, vol. 69, no. 3–4, pp. 171–180, Jan. 2007.

[22] X. Chen and S. S. Mao, “Titanium Dioxide Nanomaterials: Synthesis, Properties, Modifications, and Applications,” *Chem. Rev.*, vol. 107, no. 7, pp. 2891–2959, Jul. 2007.

[23] T. Kasuga, M. Hiramatsu, A. Hoson, T. Sekino, and K. Niihara, “Formation of Titanium Oxide Nanotube,” *Langmuir*, vol. 14, no. 12, pp. 3160–3163, Jun. 1998.

[24] C. L. Wong, Y. N. Tan, and A. R. Mohamed, “A review on the formation of

titanium nanotube photocatalysts by hydrothermal treatment,” *J. Environ. Manage.*, vol. 92, no. 7, pp. 1669–1680, Jul. 2011.

[25] K. Khoshroo, T. S. Jafarzadeh Kashi, F. Moztarzadeh, H. Eslami, and M. Tahriri, “The Influence of Calcination Temperature on the Structural and Biological Characteristics of Hydrothermally Synthesized TiO₂ Nanotube: In Vitro Study,” *Synth. React. Inorganic, Met. Nano-Metal Chem.*, vol. 46, no. 8, pp. 1189–1194, 2016.

[26] A. Ranjitha, N. Muthukumarasamy, M. Thambidurai, D. Velauthapillai, S. Agilan, and R. Balasundaraprabhu, “Effect of reaction time on the formation of TiO₂ nanotubes prepared by hydrothermal method,” *Optik (Stuttg.)*, vol. 126, no. 20, pp. 2491–2494, Oct. 2015.

[27] S. Sreekantan and L. C. Wei, “Study on the formation and photocatalytic activity of titanate nanotubes synthesized via hydrothermal method,” *J. Alloys Compd.*, vol. 490, no. 1–2, pp. 436–442, Feb. 2010.

[28] Z.-Y. Yuan and B.-L. Su, “Titanium oxide nanotubes, nanofibers and nanowires,” *Colloids Surfaces A Physicochem. Eng. Asp.*, vol. 241, no. 1–3, pp. 173–183, Jul. 2004.

[29] S.-S. Liu, C.-K. Lee, H.-C. Chen, C.-C. Wang, and L.-C. Juang, “Application of titanate nanotubes for Cu(II) ions adsorptive removal from aqueous solution,” *Chem. Eng. J.*, vol. 147, no. 2–3, pp. 188–193, Apr. 2009.

[30] D. V. Bavykin, J. M. Friedrich, and F. C. Walsh, “Protonated Titanates and TiO₂ Nanostructured Materials: Synthesis, Properties, and Applications,” *Adv. Mater.*, vol. 18, no. 21, pp. 2807–2824, Nov. 2006.

[31] “<https://nanobakt.hu/titanat-nanocso/>,” p. 2019, 2019.

[32] M. Hodos, “Titanát nanocsövek szintézise, jellemzése és egy lehetséges képződési modellje,” 2007.

[33] Q. Ai, D. Yang, Y. Li, J. Shi, X. Wang, and Z. Jiang, “Highly efficient covalent immobilization of catalase on titanate nanotubes,” *Biochem. Eng. J.*, vol. 83, no. C, pp. 8–15, 2014.

[34] S. J. Cho, H. J. Kim, J. H. Lee, H. W. Choi, H. G. Kim, H. M. Chung, and J. T. Do, “Silica coated titania nanotubes for drug delivery system,” 2010.

[35] B. Joshi, C. Regmi, D. Dhakal, G. Gyawali, and S. W. Lee, “Efficient inactivation of *Staphylococcus aureus* by silver and copper loaded photocatalytic titanate nanotubes,” *Prog. Nat. Sci. Mater. Int.*, vol. 28, no. 1, pp. 15–23, 2018.

[36] N. Khoshnood, A. Zamanian, and A. Massoudi, “Mussel-inspired surface modification of titania nanotubes as a novel drug delivery system,” *Mater. Sci. Eng. C*, vol. 77, pp. 748–754, 2017.

[37] X. Liu, P. K. Chu, and C. Ding, “Surface nano-functionalization of biomaterials,” *Mater. Sci. Eng. R*, vol. 70, no. 3–6, pp. 275–302, 2010.

[38] C. C. Torres, C. H. Campos, C. Díaz, V. A. Jiménez, F. Vidal, L. Guzmán, and J. B. Alderete, “PAMAM-grafted TiO₂ nanotubes as novel versatile materials for drug delivery applications,” *Mater. Sci. Eng. C*, vol. 65, pp. 164–171, 2016.

[39] C. Mirjolet, A. L. Papa, G. Créange, O. Raguin, C. Seigne, C. Paul, G. Truc, P. Maingon, and N. Millot, “The radiosensitization effect of titanate nanotubes as a new tool in radiation therapy for glioblastoma: A proof-of-concept,” *Radiother. Oncol.*, vol. 108, no. 1, pp. 136–142, 2013.

[40] S. Wadhwa, C. Rea, P. O’Hare, a. Mathur, S. S. Roy, P. S. M. Dunlop, J. a. Byrne, G. Burke, B. Meenan, and J. a. McLaughlin, “Comparative in vitro cytotoxicity study of carbon nanotubes and titania nanostructures on human lung epithelial cells,” *J. Hazard. Mater.*, vol. 191, no. 1–3, pp. 56–61, 2011.

[41] L. Zhao, S. Mei, W. Wang, P. K. Chu, Z. Wu, and Y. Zhang, “The role of sterilization in the cytocompatibility of titania nanotubes,” *Biomaterials*, vol. 31, no. 8,

pp. 2055–2063, 2010.

[42] F. Fenyvesi, Z. Kónya, Z. Rázga, M. Vecsernyés, P. Kása, K. Pintye-Hódi, and I. Bácskay, “Investigation of the cytotoxic effects of titanate nanotubes on Caco-2 cells,” *AAPS PharmSciTech*, vol. 15, no. 4, pp. 858–61, 2014.

[43] A. L. Papa, L. Dumont, D. Vandroux, and N. Millot, “Titanate nanotubes: Towards a novel and safer nanovector for cardiomyocytes,” *Nanotoxicology*, vol. 7, no. 6, pp. 1131–1142, 2013.

[44] S. S. Mahshid, S. Luo, L. Yang, S. Mahshid, A. Dolati, M. Ghorbani, and Q. Cai, “A Well-Dispersed Pt/Ni/TiO₂ Nanotubes Modified Electrode as an Amperometric Non-Enzymatic Glucose Biosensor,” *Sens. Lett.*, vol. 9, no. 5, pp. 1598–1605, 2012.

[45] S. Mahshid, S. Luo, L. Yang, S. S. Mahshid, M. Askari, A. Dolati, and Q. Cai, “Carbon-Pt Nanoparticles Modified TiO₂ Nanotubes for Simultaneous Detection of Dopamine and Uric Acid,” *J. Nanosci. Nanotechnol.*, vol. 11, no. 8, pp. 6668–6675, 2011.

[46] D. Sović, A. Gajović, and D. Iveković, “Bioelectrocatalytic and biosensing properties of horseradish peroxidase covalently immobilized on (3-aminopropyl)trimethoxysilane-modified titanate nanotubes,” *Electrochim. Acta*, vol. 56, no. 27, pp. 9953–9960, 2011.

[47] H. Tao, X. Wang, X. Wang, Y. Hu, Y. Ma, Y. Lu, and Z. Hu, “Construction of Uric Acid Biosensor Based on Biomimetic Titanate Nanotubes,” *J. Nanosci. Nanotechnol.*, vol. 10, no. 2, pp. 860–864, 2010.

[48] B. A. Liu, M. Wei, I. Honma, and H. Zhou, “Biosensing Properties of Titanate-Nanotube Films : Selective Detection of Dopamine in the Presence of Ascorbate and Uric Acid *,” pp. 371–376, 2006.

[49] S. Beke, R. Barengi, B. Farkas, I. Romano, L. Korösi, S. Scaglione, and F. Brandi, “Improved cell activity on biodegradable photopolymer scaffolds using titanate nanotube coatings,” *Mater. Sci. Eng. C*, vol. 44, no. November, pp. 38–43, 2014.

[50] D. P. Bhattarai, S. Shrestha, B. K. Shrestha, C. H. Park, and C. S. Kim, “A controlled surface geometry of polyaniline doped titania nanotubes biointerface for accelerating MC3T3-E1 cells growth in bone tissue engineering,” *Chem. Eng. J.*, vol. 350, no. October, pp. 57–68, 2018.

[51] K. S. Brammer, C. J. Frandsen, and S. Jin, “TiO₂ nanotubes for bone regeneration,” vol. 30, no. 6, 2012.

[52] C. Chiang, S. Chiou, W. Yang, and M. Hsu, “Formation of TiO₂ nano-network on titanium surface increases the human cell growth,” vol. 5, pp. 1022–1029, 2009.

[53] C. X. Cui, X. Gao, Y. M. Qi, S. J. Liu, and J. B. Sun, “Microstructure and antibacterial property of in situ TiO₂ nanotube layers / titanium biocomposites,” vol. 8, pp. 178–183, 2012.

[54] H. Eslami, H. Azimi Lisar, T. S. Jafarzadeh Kashi, M. Tahriri, M. Ansari, T. Rafiei, F. Bastami, A. Shahin-Shamsabadi, F. Mashhadi Abbas, and L. Tayebi, “Poly(lactic-co-glycolic acid)(PLGA)/TiO₂ nanotube bioactive composite as a novel scaffold for bone tissue engineering: In vitro and in vivo studies,” *Biologicals*, vol. 53, no. May, pp. 51–62, 2018.

[55] E. Kato, K. Sakurai, and M. Yamada, “Periodontal-like gingival connective tissue attachment on titanium surface with nano-ordered spikes and pores created by alkali-heat treatment,” *Dent. Mater.*, pp. 2–9, 2015.

[56] S. Y. Kim, Y. K. Kim, Y. S. Jang, I. S. Park, S. J. Lee, J. G. Jeon, and M. H. Lee, “Bioactive effect of alkali-heat treated TiO₂ nanotubes by water or acid treatment,” *Surf. Coatings Technol.*, vol. 303, no. October, pp. 256–267, 2016.

- [57] A. Kodama, S. Bauer, A. Komatsu, H. Asoh, S. Ono, and P. Schmuki, "Bioactivation of titanium surfaces using coatings of TiO₂ nanotubes rapidly pre-loaded with synthetic hydroxyapatite," *Acta Biomater.*, vol. 5, no. 6, pp. 2322–2330, 2009.
- [58] J. Kunze, M. Lenka, J. M. Macak, P. Greil, P. Schmuki, and A. M. Frank, "Time-dependent growth of biomimetic apatite on anodic TiO₂ nanotubes," vol. 53, pp. 6995–7003, 2008.
- [59] Q. Lin, D. Huang, J. Du, Y. Wei, Y. Hu, X. Lian, X. Xie, W. Chen, and Y. S. Zhang, "Nano-hydroxyapatite crystal formation based on calcified TiO₂ nanotube arrays," *Appl. Surf. Sci.*, vol. 478, pp. 237–246, 2019.
- [60] S. Minagar, Y. Li, C. C. Berndt, and C. Wen, "The influence of titania-zirconia-zirconium titanate nanotube characteristics on osteoblast cell adhesion," *Acta Biomater.*, vol. 12, no. 1, pp. 281–289, 2015.
- [61] M. P. Neupane, I. S. Park, T. S. Bae, H. K. Yi, F. Watari, and M. H. Lee, "Biocompatibility of TiO₂ nanotubes fabricated on Ti using different surfactant additives in electrolyte," *Mater. Chem. Phys.*, vol. 134, no. 1, pp. 536–541, 2012.
- [62] Y. Parcharoen, P. Kajitvichyanukul, S. Sirivisoot, and P. Termsuksawad, "Hydroxyapatite electrodeposition on anodized titanium nanotubes for orthopedic applications," *Appl. Surf. Sci.*, vol. 311, no. August, pp. 54–61, 2014.
- [63] J. Peng, X. Zhang, Z. Li, Y. Liu, and X. Yang, "Titania nanotube delivery fetal bovine serum for enhancing MC3T3-E1 activity and osteogenic gene expression," *Mater. Sci. Eng. C*, vol. 56, pp. 438–443, 2015.
- [64] A. Pittrof, S. Bauer, and P. Schmuki, "Acta Biomaterialia Micropatterned TiO₂ nanotube surfaces for site-selective nucleation of hydroxyapatite from simulated body fluid," *Acta Biomater.*, vol. 7, no. 1, pp. 424–431, 2011.
- [65] H. Qiao, Q. Zou, C. Yuan, X. Zhang, S. Han, Z. Wang, X. Bu, H. Tang, and Y. Huang, "Composite coatings of lanthanum-doped fluor-hydroxyapatite and a layer of strontium titanate nanotubes: fabrication, bio-corrosion resistance, cytocompatibility and osteogenic differentiation," *Ceram. Int.*, vol. 44, no. 14, pp. 16632–16646, 2018.
- [66] I. Roman, R. Doina, M. Soare, C. Fratila, E. Krasicka-cydzik, M. Stan, and A. Dinischiotu, "Titanium dioxide nanotube films Preparation, characterization and electrochemical biosensitivity towards alkaline phosphatase," vol. 37, pp. 374–382, 2014.
- [67] B. S. Smith, S. Yoriya, T. Johnson, and K. C. Popat, "Dermal fibroblast and epidermal keratinocyte functionality on titania nanotube arrays," *Acta Biomater.*, vol. 7, no. 6, pp. 2686–2696, 2011.
- [68] K. Subramani and W. Ahmed, "Titanium Nanotubes as Carriers of Osteogenic Growth Factors and Antibacterial Drugs for Applications in Dental Implantology," *Emerg. Nanotechnologies Dent.*, pp. 103–111, 2012.
- [69] K. Vasilev, Z. Poh, K. Kant, J. Chan, A. Micheltmore, and D. Losic, "Biomaterials Tailoring the surface functionalities of titania nanotube arrays," *Biomaterials*, vol. 31, no. 3, pp. 532–540, 2010.
- [70] C. Wang, Y. Bai, Y. Bai, J. Gao, and W. Ma, "Enhancement of corrosion resistance and bioactivity of titanium by Au nanoparticle-loaded TiO₂ nanotube layer," *Surf. Coatings Technol.*, vol. 286, pp. 327–334, 2016.
- [71] W. Yu, C. Qian, X. Jiang, F. Zhang, and W. Weng, "Mechanisms of stem cell osteogenic differentiation on TiO₂ nanotubes," *Colloids Surfaces B Biointerfaces*, vol. 136, pp. 779–785, 2015.
- [72] K. Gulati, S. Ramakrishnan, M. Sinn, G. J. Atkins, D. M. Findlay, and D. Losic, "Acta Biomaterialia Biocompatible polymer coating of titania nanotube arrays for improved drug elution and osteoblast adhesion," *Acta Biomater.*, vol. 8, no. 1, pp. 449–456, 2012.

- [73] M. S. Aw and D. Losic, "Ultrasound enhanced release of therapeutics from drug-releasing implants based on titania nanotube arrays," *Int. J. Pharm.*, vol. 443, no. 1–2, pp. 154–162, 2013.
- [74] P. Chennell, E. Feschet-Chassot, T. Devers, K. O. Awitor, S. Descamps, and V. Sautou, "In vitro evaluation of TiO₂ nanotubes as cefuroxime carriers on orthopaedic implants for the prevention of periprosthetic joint infections," *Int. J. Pharm.*, vol. 455, no. 1–2, pp. 298–305, 2013.
- [75] A. L. Doadrio, A. Conde, M. A. Arenas, J. M. Hernández-López, J. J. de Damborenea, C. Pérez-Jorge, J. Esteban, and M. Vallet-Regí, "Use of anodized titanium alloy as drug carrier: Ibuprofen as model of drug releasing," *Int. J. Pharm.*, vol. 492, no. 1–2, pp. 207–12, Aug. 2015.
- [76] W. Feng, Z. Geng, Z. Li, Z. Cui, S. Zhu, Y. Liang, Y. Liu, R. Wang, and X. Yang, "Controlled release behaviour and antibacterial effects of antibiotic-loaded titania nanotubes," *Mater. Sci. Eng. C*, vol. 62, pp. 105–112, 2016.
- [77] Y. Hu, K. Cai, Z. Luo, D. Xu, D. Xie, Y. Huang, W. Yang, and P. Liu, "Acta Biomaterialia TiO₂ nanotubes as drug nanoreservoirs for the regulation of mobility and differentiation of mesenchymal stem cells," *Acta Biomater.*, vol. 8, no. 1, pp. 439–448, 2012.
- [78] P. Huo, Kaifu; Xu,Na; Fu Jijiang; K.Chu, "Chapter 17 - Bioactive inorganic-ion-doped titania nanotube coatings on bone implants with enhanced osteogenic activity and antibacterial properties," p. 2019, 2019.
- [79] K. Indira, U. Kamachimudali, and N. Rajendran, "Applied Surface Science In vitro bioactivity and corrosion resistance of Zr incorporated TiO₂ nanotube arrays for orthopaedic applications," *Appl. Surf. Sci.*, vol. 316, pp. 264–275, 2014.
- [80] K. Indira, U. K. Mudali, and N. Rajendran, "In-vitro biocompatibility and corrosion resistance of strontium incorporated TiO₂ nanotube arrays for orthopaedic applications," *J. Biomater. Appl.*, vol. 316, pp. 264–275, 2013.
- [81] A. Roguska, M. Pisarek, A. Belcarz, L. Marcon, M. Holdynski, M. Andrzejczuk, and M. Janik-Czachor, "Improvement of the bio-functional properties of TiO₂ nanotubes," *Appl. Surf. Sci.*, vol. 388, pp. 775–785, 2016.
- [82] L. Zhao, H. Wang, K. Huo, X. Zhang, W. Wang, Y. Zhang, Z. Wu, and P. K. Chu, "Biomaterials The osteogenic activity of strontium loaded titania nanotube arrays on titanium substrates," *Biomaterials*, pp. 1–11, 2012.
- [83] X. Chen, K. Cai, J. Fang, M. Lai, Y. Hou, J. Li, Z. Luo, Y. Hu, and L. Tang, "Fabrication of selenium-deposited and chitosan-coated titania nanotubes with anticancer and antibacterial properties," *Colloids Surfaces B Biointerfaces*, vol. 103, pp. 149–157, 2013.
- [84] T. Kumeria, H. Mon, M. S. Aw, K. Gulati, A. Santos, H. J. Griesser, and D. Losic, "Advanced biopolymer-coated drug-releasing titania nanotubes (TNTs) implants with simultaneously enhanced osteoblast adhesion and antibacterial properties," *Colloids Surf. B. Biointerfaces*, vol. 130, pp. 255–63, Jun. 2015.
- [85] M. Science, "Preparation of TiO₂ nanotubes / mesoporous calcium silicate composites with controllable drug release," vol. 67, no. October, 2016.
- [86] T. Wang, Z. Weng, X. Liu, K. W. K. Yeung, H. Pan, and S. Wu, "Controlled release and biocompatibility of polymer/titania nanotube array system on titanium implants," *Bioact. Mater.*, vol. 2, no. 1, pp. 44–50, 2017.
- [87] Y. Zhang, L. Chen, C. Liu, X. Feng, L. Wei, and L. Shao, "Self-assembly chitosan/gelatin composite coating on icariin-modified TiO₂ nanotubes for the regulation of osteoblast bioactivity," *Mater. Des.*, vol. 92, pp. 471–479, 2016.
- [88] S. J. Cho, H. J. Kim, J. H. Lee, H. W. Choi, H. G. Kim, H. M. Chung, and J. T.

Do, "Silica coated titania nanotubes for drug delivery system," *Mater. Lett.*, vol. 64, no. 15, pp. 1664–1667, 2010.

[89] S. Sruthi, A. Loiseau, J. Boudon, F. Sallem, L. Maurizi, P. V. Mohanan, G. Lizard, and N. Millot, "In vitro interaction and biocompatibility of titanate nanotubes with microglial cells," *Toxicol. Appl. Pharmacol.*, vol. 353, no. August, pp. 74–86, 2018.

[90] M. C., B. J., L. A., C. S., B. R., O. A., C. B., M. E., J. P.A., M. N., and C. G., "Docetaxel-titanate nanotubes enhance radiosensitivity in an androgen-independent prostate cancer model," *Int. J. Nanomedicine*, vol. 12, no. 3, pp. 6357–6364, 2017.

[91] M. Ray, S. Chatterjee, T. Das, S. Bhattacharyya, P. Ayyub, and S. Mazumdar, "Conjugation of cytochrome c with hydrogen titanate nanotubes: Novel conformational state with implications for apoptosis," *Nanotechnology*, vol. 22, no. 41, p. 2, 2011.

[92] S. Sruthi, A. Loiseau, J. Boudon, F. Sallem, L. Maurizi, P. V. Mohanan, G. Lizard, and N. Millot, "In vitro interaction and biocompatibility of titanate nanotubes with microglial cells," *Toxicol. Appl. Pharmacol.*, vol. 353, pp. 74–86, 2018.

[93] T. Baati, B. B. Kefi, A. Aouane, L. Njim, F. Chaspoul, V. Heresanu, A. Kerkeni, F. Neffati, and M. Hammami, "Biocompatible titanate nanotubes with high loading capacity of genistein: Cytotoxicity study and anti-migratory effect on U87-MG cancer cell lines," *RSC Adv.*, vol. 6, no. 103, pp. 101688–101696, 2016.

[94] A. Loiseau, J. Boudon, C. Mirjolet, G. Créhange, and N. Millot, "Taxane-Grafted Metal-Oxide Nanoparticles as a New Theranostic Tool against Cancer: The Promising Example of Docetaxel-Functionalized Titanate Nanotubes on Prostate Tumors," *Adv. Healthc. Mater.*, vol. 6, no. 16, p. 70, 2017.

[95] A. Elhissi and D. Phoenix, "Some approaches to large-scale manufacturing of liposomes," *Emerg. Nanotechnologies Manuf.*, pp. 402–417, Jan. 2015.

[96] B. Sipos, K. Pintye-Hódi, Z. Kónya, A. Kelemen, G. Regdon, and T. Sovány, "Physicochemical characterisation and investigation of the bonding mechanisms of API-titanate nanotube composites as new drug carrier systems," *Int. J. Pharm.*, vol. 518, no. 1, pp. 119–129, 2017.

[97] United States Pharmacopeia, "USP Powder Flow," *Stage 6 Harmon.*, vol. 30(60), no. 6, p. 7, 2016.

[98] B. Sipos, G. Regdon, Z. Kónya, K. Pintye-Hódi, and T. Sovány, "Comparative study on the rheological properties and tablettability of various APIs and their composites with titanate nanotubes," *Powder Technol.*, vol. 321, pp. 419–427, Nov. 2017.

[99] B. Sipos, K. Pintye-Hódi, G. Regdon, Z. Kónya, M. Viana, and T. Sovány, "Investigation of the Compressibility and Compactibility of Titanate Nanotube-API Composites," *Materials (Basel)*, vol. 11, no. 12, p. 2582, Dec. 2018.

[100] C. B. Ferster and B. F. Skinner, "Pharmaceutical Technical procedures," *Eur. Pharmacop.*, no. 1, pp. 19–43, 1957.

ACKNOWLEDGMENT

First of all, I would like to express my warmest thanks to my supervisors, **Dr. Tamás Sovány** and **Dr. Géza Regdon jr.** for their guidance, encouragement and continuous help during my Ph.D. studies.

I am also very grateful to **Prof. Dr. Klára Pintye-Hódi** for her support and valuable advice in my research work.

I would like to thank **Dr. Ildikó Csóka** and **Prof. Dr. Piroska Szabó-Révész**, present and former head of the Pharmaceutical Technology Educational Program of the Doctoral School of Pharmaceutical Sciences, and present and former head of the Institute of Pharmaceutical Technology and Regulatory Affairs for providing me with the opportunity to complete my work in the department.

I am also thankful to my colleagues in the solid dosage form team, **Ildikó Vigh** and **Gabriella Molnár** for their technical assistance in my experimental work.

I would like to express my gratitude to **Mme Marilène Viana** (University of Limoges, Department of Pharmaceutical Technology) for providing me with the possibility to work in her department and for her useful advice and instructions.

Finally, my biggest thanks go to **my family** and **my friends** who believed in me and encouraged me all along my studies. I am deeply grateful for their constant support and love.

NYILATKOZAT SAJÁT MUNKÁRÓL

Név:

Sipos Barbara

Doktori értekezés címe:

Investigation of physicochemical characteristics and tablettability of titanate nanotube-active drug composites

Én, **Sipos Barbara**, teljes felelősségem tudatában kijelentem, hogy a Szegedi Tudományegyetem Gyógyszertudományok Doktori Iskolában elkészített doktori (Ph.D.) disszertációm saját kutatási eredményeimen alapul. Kutatómunkám, eredményeim publikálása, valamint disszertációm megírása során a Magyar Tudományos Akadémia Tudományetikai Kódexében lefektetett alapelvek és ajánlások szerint jártam el.

Budapest, 2019.05.27.



Sipos Barbara